Marine and Petroleum Geology xxx (2016) xxx-xxx

Contents lists available at ScienceDirect

Marine and Petroleum Geology

journal homepage: www.elsevier.com

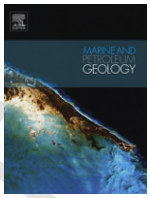

Research paper

Assessment of thermal evolution of Paleozoic successions of the Holy Cross Mountains (Poland)

A. Schito [a, *], S. Corrado [a], M. Trolese [a], L. Aldega [b], C. Caricchi [c], S. Cirilli [d], D. Grigo [e], A. Guedes [f], C. Romano [a], A. Spina [d], B. Valentim [f]

[a] Università degli Studi di Roma Tre, Dipartimento di Scienze, Sezione di Scienze Geologiche, Largo San Leonardo Murialdo 1, 00146, Rome, Italy
[b] Sapienza Università di Roma, Dipartimento di Scienze della Terra, Piazzale Aldo Moro 5, 00185, Rome, Italy
[c] INGV, Via di Vigna Murata 605, 00100, Rome, Italy
[d] Università degli Studi di Perugia, Dipartimento di Fisica e Geologia, Via Alessandro Pascoli, 06123, Perugia, PG, Italy
[e] Eni SpA - Exploration & Production Division, Via Emilia, San Donato Milanese, MI, 20097, Italy
[f] Instituto de Ciências da Terra (Pólo da FCUP), Departamento de Geociências, Ambiente e Ordenamento do Território, Faculdade de Ciências, Universidade do Porto, 4169-007, Porto, Portugal

ARTICLE INFO

Article history:
Received 27 July 2016
Received in revised form 7 October 2016
Accepted 15 November 2016
Available online xxx

Keywords:
Paleozoic source rocks
Thermal maturity
Vitrinite and organoclast reflectance
Clay mineralogy
Raman spectroscopy
Palynomorph darkness index
Holy Cross Mountains

ABSTRACT

Poland is considered the most prospective country for shale gas production in Europe. Hydrocarbon generation/expulsion scenarios, drawn in the latest intensive exploration phases, tend to overestimate maturation levels when compared with brand new data acquired after recent drillings. We tested an integrated workflow to correlate published and original thermal maturity datasets for the Paleozoic to Jurassic successions cropping out in the Holy Cross Mountains. These successions, when preserved in subsurface, host the major source rocks in the area. The application of the workflow allowed us to highlight the burial and thermal evolutionary scenarios of the two tectono-stratigraphic blocks of the Holy Cross Mountains (Łysogóry and Kielce blocks) and to propose this approach as a tool for reducing levels of uncertainty in thermal maturity assessment of Paleozoic successions worldwide. In particular, published datasets including colour alteration indexes of Paleozoic microfossils (conodont, acritarchs) and vitrinite and graptolite reflectance data, show differences in levels of thermal maturity for the Łysogóry (mid mature to overmature) and Kielce (immature to late mature) blocks. Original data, derived from optical analysis, pyrolysis, and Raman spectroscopy on kerogen, and X-Ray diffraction on fine-grained sediments, mostly confirm and integrate published data distribution. 1D thermal models, constrained by these data, show burial and exhumation events of different magnitude, during the Late Cretaceous, for the Łysogóry (maximum burial depths of 9 km) and Kielce (burial depths of 6 km) blocks that have been related to the Holy Cross Fault polyphase activity. In the end, Palynomorph Darkness Index and Raman spectroscopy on kerogen, for Llandoverian and Cambrian rocks, turned out to be promising tools for assessing thermal maturity of Paleozoic organic facies devoid of vitrinite macerals.

1. Introduction

Reliable assessment of thermal maturity of sedimentary successions is crucial for evaluating hydrocarbon (HC) generation/expulsion scenarios. Uncertainties in thermal maturity modelling can affect decisions on the development of prospects, especially when aimed at exploring unconventional targets (Hackley and Cardott, 2016). In particular, this happens for lower Paleozoic source rocks, because they are devoid of vitrinite macerals that are, by far, the most reliable organic particles used to assess thermal maturity in the ranges of oil and gas generation (Taylor et al., 1998). However, when vitrinite is absent, reflectance measurements and further chemical investigations can be determined on organoclasts of marine origin (e.g., scolecodonts, chitinozoans, and particularly graptolites, cfr. Bertrand, 1990; Bertrand and Heroux, 1987; Goodarzi and Norford, 1987, 1989; Tricker et al., 1992; Caricchi et al., 2016; Hackley and Cardott, 2016).

During the last years, a great interest in unconventional resources has grown in Poland, which has been envisaged as the most prospective country in Europe for exploration of shale gas (SHIP website, http://www.shale-gas-information-platform.org/). In Poland, the main targets for shale-gas and shale-oil exploration are represented by Lower Paleozoic successions preserved in the subsurface in a wide belt (the "Golden belt", Fig. 1), extending from the Baltic Sea to the NW, to the Ukraine border to the SE, between the Baltic and the Lublin basins. However, levels of thermal maturity for the source rocks in the "Golden belt" have been often overestimated, as pointed out by Caricchi et al. (2016) and Jäger (2016), who concluded that most of the expected gas targets are actually in the oil generation stages.

In this framework, it is crucial to test a new rationale to compare and integrate published and original datasets, especially in areas where exploration has been ongoing since long ago. Holy Cross Mountains (HCM) in Central Poland, provide a unique opportunity to

* Corresponding author.
Email address: andrea.schito@uniroma3.it (A. Schito)

http://dx.doi.org/10.1016/j.marpetgeo.2016.11.016
0264-8172/

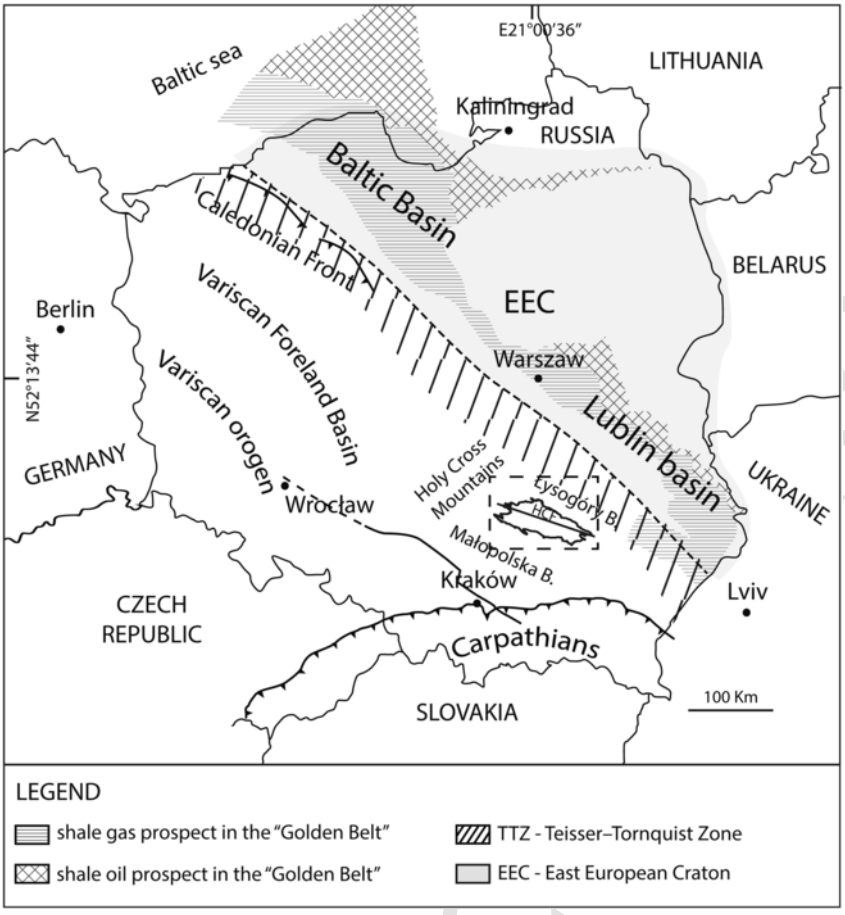

Fig. 1. Location of the study area (dashed rectangle) and shale and oil prospects in Poland, http://www.ogj.com. Acronyms: HCF = Holy Cross Fault; TTZ = Teisseyre-Tornquist zone.

study outcropping Paleozoic successions that are analogous to those preserved in subsurface along the "Golden Belt" (Figs. 1 and 2).

In the HCM, located to the East of the Teisseyre-Tornquist Zone (TTZ, Fig. 1), well preserved outcrops of Cambrian to Carboniferous sedimentary rocks are exposed, as a results of a relevant exhumation event at the end of Mesozoic times. Several papers (Belka, 1990; Narkiewicz, 2002; Szczepanik, 1997, 2001) have unraveled the complex burial and thermal history of the HCM using different datasets

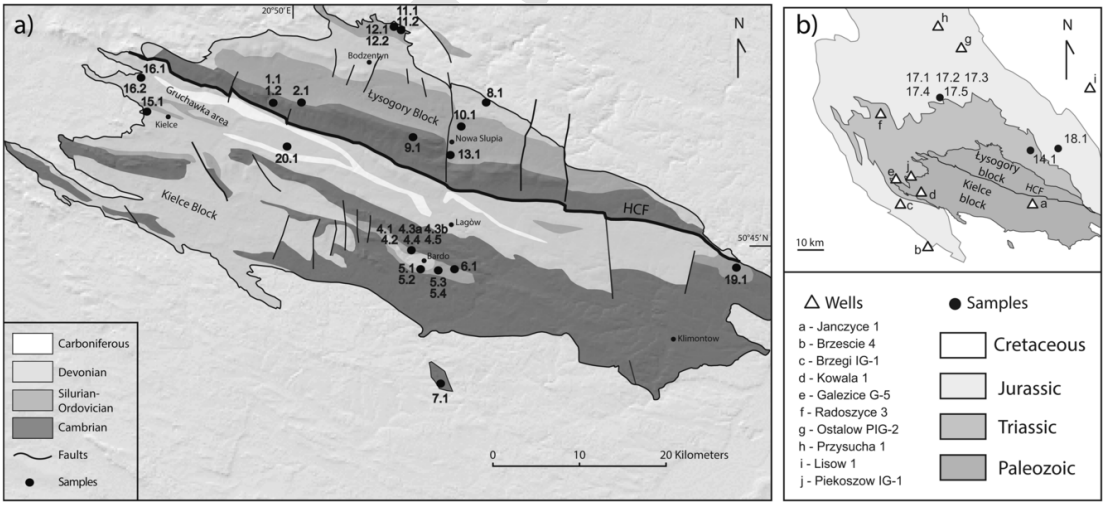

Fig. 2. (a) Geological map of the Paleozoic successions in the HCM with sampling location (modified and redrawn after Konon, 2007). Black dots refers to Paleozoic samples; (b) simplified sketch map of the Mesozoic cover in the HCM area showing sampling and wells location. Acronyms: HCF = Holy Cross Fault; HCM = Holy Cross Mountains. Black dots refer to Mesozoic samples, white triangles refer to the wells.

of thermal maturity indicators (e.g., Conodont Alteration Index - CAI; Thermal Alteration Index - TAI and vitrinite reflectance - R_o% and other organoclasts (e.g., graptolite) and/or vitrinite-like fragments reflectance – $R_{o\ org}$%), but a comprehensive and fully accepted burial vs exhumation model has not yet been elaborated. In particular, major uncertainties derive from the lack of a widely accepted correlation among thermal indicators (e.g., TAI, CAI, R_o%, $R_{o\ org}$%) against maximum paleotemperatures that could lead to contrasting interpretations in the assessment of maturation patterns and timing of hydrocarbon generation of Lower Silurian potential source rocks (Belka, 1990; Marynowski et al., 2001; Narkiewicz, 2002 ; Poprawa et al., 2005; Narkiewicz and Narkiewicz, 2010). Lower Silurian source rocks have been recently investigated by means of organic matter optical analyses and Rock-Eval pyrolysis (Malec et al., 2010; Mustafa et al., 2015; Smolarek et al., 2014), but these data have not been employed as constraints for thermal modelling.

In this paper, available thermal maturity data from literature have been revised and integrated with original thermal maturity data derived from the analyses of the organic (e.g., T_{max} from Rock-Eval pyrolysis, and vitrinite and other organoclasts reflectance, e.g. R_o%, $R_{o\ org}$%) and inorganic fraction (e.g., illite content in mixed layers illite-smectite) of sediments.

This multi-method approach allowed us to highlight the burial and thermal evolutionary scenarios of the two tectono-stratigraphic blocks of the HCM (Łysogòry and Kielce blocks; Fig. 2). Furthermore, the integration of different thermal indicators from the organic and inorganic portion of sediments is proposed to reduce levels of uncertainty in thermal maturity assessment, and can be successfully applied to similar Paleozoic source rocks successions in Poland and worldwide.

2. Geological setting

The HCM are organized into two distinct tectono-stratigraphic blocks: the southern block (Kielce block, that is a part of the Małopolska block) and the northern block (Łysogòry block), bounded by a deep-seated regional lineament, at least 75 km long, known as the Holy Cross Fault (HCF, Figs. 1 and 2) whose kinematic evolution is still matter of debate (Dadlez, 2001; Kutek, 2001).

Cambrian sediments, exposed in both blocks (Fig. 3), are made up of shales, evolving to quartzarenites and sandstones (Narkiewicz, 2002) deposited along the SW passive margin of the Baltica continent (Mizerski, 2004).

Ordovician successions are composed of clayey and silty marine deposits and are overlain by Llandoverian-Wenlockian graptolitic black shales (Kozłowski, 2008). Lower Silurian shales are covered by Ludfordian greywackes composed of the Niewachlów Beds in the Kielce region (Fig. 3; Kozłowski et al., 2014) and the Trzcianka, Trochowiny and Winnica Formations in the Łysogóry block (Fig. 3, Kozłowski, 2008). On the other hand, the Upper Silurian interval in the Kielce region is represented by sandstones and locally by the Miedziana Góra conglomerates (Kozłowski et al., 2014, Fig. 3), whereas, it is composed of a thick succession of clastic sediments in the Łysogòry block that represents a continuous Late Ludlovian-Lochkovian deposition in the Caledonian foreland basin (Narkiewicz, 2002). The Lower Devonian successions (Pragian-Emsian) are constituted by terrigenous sediments with interlayered organic matter rich black shales (Marynowski et al., 2001) whereas the middle and Upper Devonian rocks are shallow water marine carbonates (Narkiewicz and Narkiewicz, 2010). Lower Carboniferous marine marly and clayey lithotypes crop out at the core of Variscan folds in the northern part of the Kielce block, close to the HCF (Fig. 2).

Facies and thickness variations between the two blocks have been related, according to Dadlez et al. (1994) and Narkiewicz (2002), to their different paleogeographic position in Lower Paleozoic times; whereas, according to Mizerski (2004), Jaworowski and Sikorska (2006) and Schätz et al. (2006), these variations could be related to differential amounts of vertical motion along the HCF.

The role of different orogenic cycles affecting the Cambrian to Carboniferous succession of the HCM is still matter of debate. The primary role played by the Variscan deformation to explain the present day tectonic setting has been widely recognized (Lamarche et al., 1999; Mizerski, 2004) with a pre-Late Carboniferous compression causing a polyphase folding associated with a dominant N-S to NNW-SSE shortening (Lamarche et al., 1999). In addition, an Early Caledonian deformation was detected by Gągała (2015) in the Lower and Middle Cambrian rocks in the Kielce block, but not all authors (e.g., Lamarche et al., 1999; Konon, 2007) agree with this piece of evidence. During Late Permian and Mesozoic times, the HCM were part of the Polish Rift Basin (Kutek and Głazek, 1972; Kutek, 2001; Lamarche et al., 1999; Mizerski, 2004). As a consequence, in the Łysogóry and Kielce blocks, the Cambrian to Devonian/Carboniferous successions were unconformably covered by a Late Permian-Early Triassic continental clastic succession (Konon, 2004; Kozłowski, 2008), that evolved to marine sediments from Late Triassic up to Late Cretaceous (Konon, 2004). Upper Permian-Mesozoic succession records a complex subsidence history ruled by an initial Late Permian-Early Triassic crustal thinning that was followed by two episodes of tectonic subsidence during the Oxfordian-Kimmeridgian and the Cenomanian (Lamarche et al., 1999; Konon, 2004). Since the Maastrichtian and during Paleocene times (Dadlez et al., 1994), the Laramide basin inversion led to the formation of the Mid-Polish Anticlinorium (Kutek, 2001) and the exhumation of Paleozoic strata (Konon, 2004; Mizerski, 2004).

3. Materials and methods

3.1. Materials

A suite of 28 samples for X-ray diffraction analyses of fine-grained sediments and optical, TOC and pyrolysis analyses of kerogen, is from Cambrian to Devonian shaly, silty and organic matter rich beds (Fig. 2a and Table 1). Seven further samples pertain to the Mesozoic succession cropping out to the north of the Łysogóry block (Fig. 2b).

Cambrian layers were collected from brownish siltstones in the southern part of the HCM (7.1, Fig. 2) and close to the HCF where black shales (1.1 and 1.2) interbedded with shaly mudstones and limestones, crop out.

Upper Ordovician (5.4, 6.1) and Llandoverian (5.1, 5.2, 5.3) samples in the Kielce block come from shales collected in the southern limb of the Bardo syncline.

Silurian graptolitic shales and mudstones were collected along the northern limb of the Bardo syncline (4.1, 4.2, 4.3a, 4.3b, 4.4 and 4.5) and in the western part of the Kielce region (19.1). In the Łysogóry block, samples are from the Bodzentyn and Nowa Slupia areas (Fig. 2a) where the Ludlow-Přídolí Winnica Formation (10.1), the lower Ludlow Trzcianka Formation (12.1, 12.2 and 13.1) and the upper Ludlow Trochowiny Formation (11.1 and 11.2) crop out.

Devonian samples come from shaly intervals from the Szydłówek Beds and the overlying Kostomłoty Beds collected near the Gruchawka area (16.1, 16.2), in the Kostomłoty hill (15.1) and to the south-east of Kielce village (20.1). In the Łysogóry block, Devonian

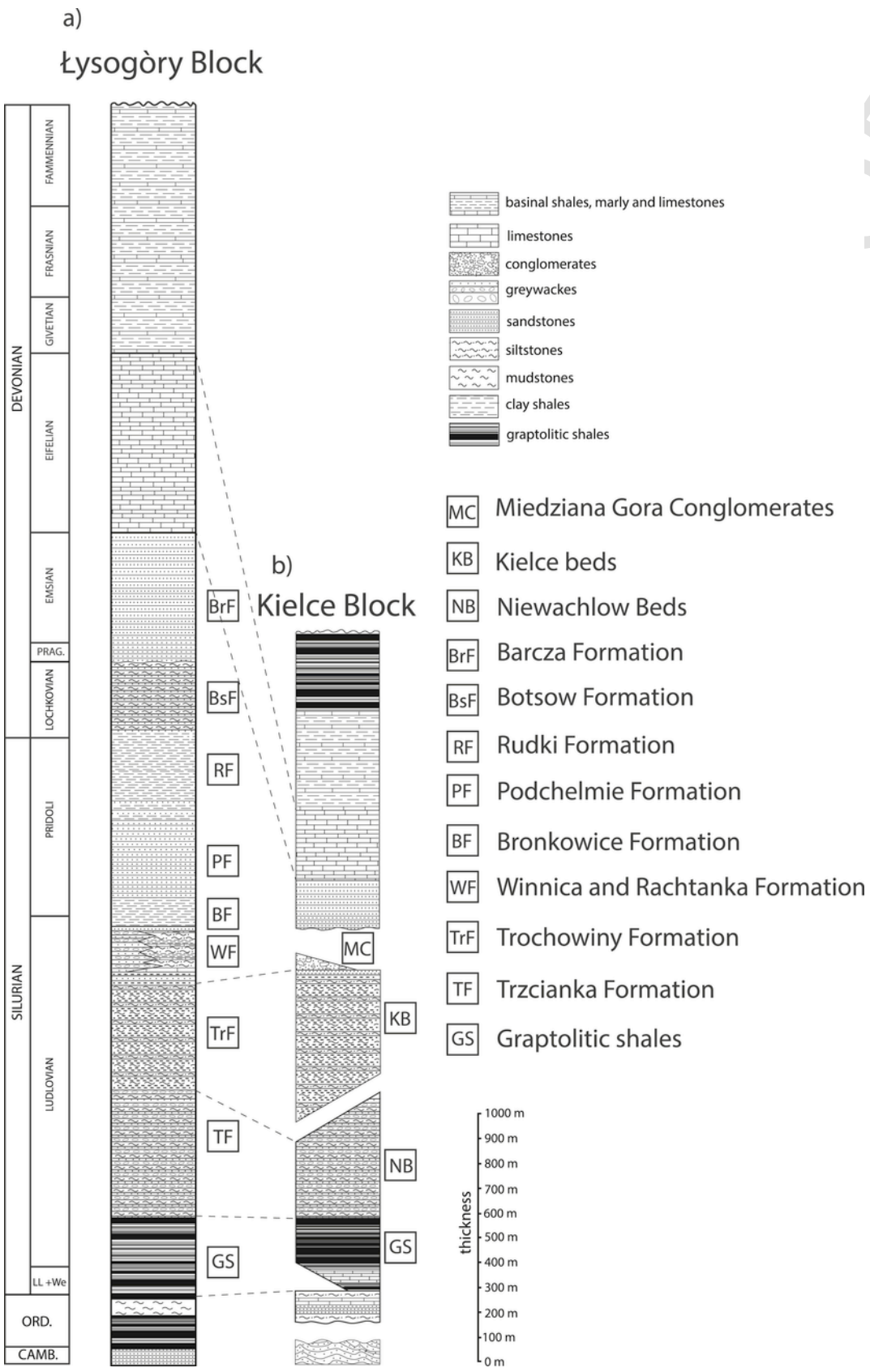

Fig. 3. Stratigraphy of the Paleozoic successions in the Łysogory (a) and Kielce blocks (b). Modified and redrawn after Kozłowski (2008) and Gągała (2015).

Table 1
Summary of sampling information (coordinates, ages, tectonic block and lithology). Sampling sites are plotted in Fig. 2 a and b. In bold: Kielce block samples; in roman: Łysogory block samples; in italics: Mesozoic samples.

Samples	Coordinates (Lat-Long)	Formation	Age	Block	Lithologies
CAMBRIAN					
7.1	**N50° 36′ 24.2″, E20° 04′ 23.0″**		**Lower Cambrian**	**Kielce**	**Siltstones**
1.1	N50° 53′ 41.2″, E20° 47′ 24.5″		Upper Cambrian	Łysogory	Black shales
1.2	N50° 53′ 43.9″, E20° 47′ 34.2″		Upper Cambrian	Łysogory	Black shales
ORDOVICIAN					
6.1	**N50° 43′ 13.3″, E21° 04′ 46.2″**		**Upper Ordovician**	**Kielce**	**Shales**
5.4	**N50° 43′ 27.4″, E21° 03′ 31.2″**	**Zalesie**	**Upper Ordovician**	**Kielce**	**Shales**
SILURIAN					
19.1	**N50° 44′ 24.8″, E21° 33′ 49.9″**		**Llandoverian**	**Kielce**	**Shales**
5.1	**N50° 43′ 27.5″, E21° 03′ 02.5″**	**Bardo**	**Llandoverian**	**Kielce**	**Shales**
5.2	**N50° 43′ 27.5″, E21° 03′ 02.5″**	**Bardo**	**Llandoverian**	**Kielce**	**Shales**
5.3	**N50° 43′ 28.4″, E21° 03′ 36.6″**	**Bardo**	**Llandoverian**	**Kielce**	**Shales**
4.5	**N50° 44′ 46.8″, E21° 02′ 14.6″**		**Wenlock**	**Kielce**	**Shales**
4.4	**N50° 44′ 43.3″, E21° 02′ 00.3″**		**Wenlock**	**Kielce**	**Mudstones**
4.3b	**N50° 44′ 49.3″, E21° 01′ 58.0″**		**Ludlowian**	**Kielce**	**Mudstones**
4.3a	**N50° 44′ 49.3″, E21° 01′ 58.0″**		**Ludlowian**	**Kielce**	**Mudstones**
4.2	**N50° 44′ 49.4″, E21° 01′ 55.5″**		**Ludlowian**	**Kielce**	**Mudstones**
4.1	**N50° 44′ 48.9″, E21° 01′ 50.5″**		**Ludlowian**	**Kielce**	**Mudstones**
13.1	N50° 50′ 34.8″, E21° 05′ 13.6″	Trzcianka	Ludlowian	Łysogory	Shales
12.1	N50° 58′ 43.5″, E21° 00′ 11.9″	Trzcianka	Ludlowian	Łysogory	Shales
12.2	N50° 58′ 43.5″, E21° 00′ 11.9″	Trzcianka	Ludlowian	Łysogory	Shales
11.1	N50° 58′ 39.6″, E21° 00′ 46.3″	Trochowiny	Ludlowian	Łysogory	Shales
11.2	N50° 58′ 39.6″, E21° 00′ 46.3″	Trochowiny	Ludlowian	Łysogory	Shales
10.1	N50° 52′ 23.0″, E21° 06′ 15.7″	Winnica	Ludlowian	Łysogory	Shales
DEVONIAN					
8.1	N50° 53′ 41.2″, E21° 09′ 30.6″		Eifelian	Łysogory	Mudstones
16.1	**N50° 55′ 24.5″, E20° 34′ 48.7″**	**Szydłówek**	**Givetian**	**Kielce**	**Shales**
16.2	**N50° 55′ 24.5″, E20° 34′ 48.7″**	**Szydłówek**	**Givetian**	**Kielce**	**Shales**
9.1	N50° 51′		Givetian/	Łysogory	Siltstones

Table 1 (*Continued*)

Samples	Coordinates (Lat-Long)	Formation	Age	Block	Lithologies
17.3	*N51° 08′ 49.7″, E20° 39′ 41.3″*		*Hettangian*	*Łysogory*	*Shales*
17.4	*N51° 08′ 49.7″, E20° 39′ 41.3″*		*Hettangian*	*Łysogory*	*Marly limestones*
17.5	*N51° 08′ 49.7″, E20° 39′ 41.3″*		*Hettangian*	*Łysogory*	*Sandstones*
18.1	*N50° 53′ 30.2″, E21° 21′ 36.3″*		*Hettangian*	*Łysogory*	*Silty shales*

samples (8.1, 9.1 and 2.1) are from: (i) Eifelian mudstones (ii) Givetian-Frasnian siltstones and (iii) black shales respectively (Fig. 2a).

For the Mesozoic successions, either Triassic reddish sandstones or Jurassic black shales were collected (Fig. 2b, Table 1).

3.2. Methods

3.2.1. Clay mineralogy

Clay minerals in shales and sandstone undergo diagenetic and very low-grade metamorphic reactions in response to sedimentary and/or tectonic burial. Reactions in clay minerals are irreversible under normal diagenetic and anchizonal conditions, so that exhumed sequences generally retain indices and fabrics indicative of their maximum thermal maturity and burial. Mixed layers illite-smectite (I-S) are widely used in petroleum exploration as a geothermometer, and as an indicator of the thermal evolution of sedimentary sequences (Hoffman and Hower, 1979; Pollastro, 1990; Aldega et al., 2007a, 2014; Schito et al., 2016a).

XRD analyses have been carried out with a Scintag X_1 X-ray system (CuKα radiation) at 40 kV and 45 mA. Randomly oriented whole rock powders were run in the 2–70° 2θ interval with a step size of 0.05°2θ and a counting time of 3s per step. Oriented mounts were prepared by the pipette-on-slide method and analyzed in the air-dried and ethylene-glycol solvated forms (saturation in ethylene-glycol atmosphere at room temperature for 24 h) in the 1–48°2θ and 1–30°2θ ranges respectively with a step size of 0.05°2θ and a counting time of 4 s per step.

The illite content in mixed-layer illite-smectite (%I in I-S) was determined by the Δ2θ method after decomposing the composite peaks between 9-10°2θ and 16–17°2θ (Moore and Reynolds, 1997) with Pearson VII functions.

The I-S ordering type (Reichweite parameter, R; Jagodzinski, 1949) was determined by the position of the illite 001/smectite 001 reflection between 5 and 8.5°2θ (Moore and Reynolds, 1997).

Peaks in relative close position were selected for clay mineral quantitative analysis of the <2 μm grain-size fraction in order to minimize the angle-dependent intensity effect. Composite peaks were decomposed using Pearson VII functions and the WINXRD Scintag associated program. Integrated peak areas were transformed into mineral concentration by using mineral intensity factors as a calibration constant (Moore and Reynolds, 1997).

3.2.2. Rock-Eval pyrolysis and TOC

Determination of Total organic carbon and Rock-Eval pyrolysis were carried out by a Rock-Eval 6 apparatus at ENI laboratories according to standard procedures. The Rock-Eval method (Espitalie et al., 1985) consists in estimating the petroleum potential of sedimentary rocks by heating samples in an open pyrolysis system under non-isothermal conditions. The released hydrocarbons were monitored by a flame ionization detector, forming the so-called peaks S1 (thermovaporized free hydrocarbons) and S2 (pyrolysis products from

cracking of organic matter). The method is completed by combustion (oxidation) of the residual rock recovered after pyrolysis up to 850 °C, under artificial air (N_2/O_2; 80/20). During pyrolysis and combustion, released CO and CO_2 were monitored on line by means of an infrared cell. This complementary data acquisition enabled determination of the organic (TOC) and mineral carbon content of samples.

3.2.3. Organic matter optical analyses

Vitrinite derives from thermal degradation of huminite-vitrinite group macerals (i.e., woody tissues of vascular plants) that can be dispersed in sediments (e.g., Stach et al., 1982; Teichmüller, 1987) and its transforming reactions are not reversible with exhumation and/or temperature decrease. Vitrinite reflectance is the most widely used quantitative parameter to determine levels of thermal maturity in hydrocarbon exploration, as it is correlated with thermal evolution of host sediments, and provides consistent and reliable information on maximum burial depths (Lopatin, 1971; Tissot and Welte, 1984; Barker, 1996; Sweeney and Burnham, 1990; Corrado et al., 2009, 2010a, 2010b; Meneghini et al., 2012; Carlini et al., 2013; Hackley and Cardott, 2016).

Although widely used and well known, this parameter cannot be measured on Early Paleozoic sediments, because of the absence of wooden terrestrial material until the Silurian advent of continental floras. However, in sedimentary sequences that are lacking of vitrinite macerals, thermal maturation can be evaluated measuring reflectance on marine organoclasts (e.g. graptolites) (Xianming et al., 2000; Bertrand and Malo, 2012; Petersen et al., 2013; Schmidt et al., 2015). Therefore, in this work, the organic matter maturation was determined using both vitrinite and graptolite reflectance according to ASTM D7708-14 and ASTM D2797.

Samples were prepared according to Bustin et al. (1989) standard procedure, and the vitrinite and organoclasts reflectance was measured under oil immersion (n_e 1.518, at 23 °C), with a Zeiss Axioskop 40 with a tungsten-halogen lamp (12 V, 100w), an Epiplan-Neofluar 50×/1.0 oil objective, in incident filtered (λ = 546 nm) monochromatic non-polarized light. The microscope is equipped with the MPS 200 detection system by J&M Analytik AG.

On each sample, from about 10 to 80 measurements were carried out on well-preserved or slightly fractured vitrinite or graptolite fragments and other kinds of organoclasts. Mean reflectance values were calculated from the arithmetic mean of each measurement set.

Thereafter, vitrinite reflectance equivalent values ($R_{o\ eq}$%) were obtained from graptolite and vitrinite-like fragments reflectance values using three different equations by Xianming et al. (2000), Petersen et al. (2013) and Schmidt et al. (2015).

These formulas are:

$R_{o\ eq}\% = 1.26\ R_{o\ org}\% + 0.21$ (when $R_{o\ org}\% < 0.75$, Xianming et al., 2000, Eq. 1)

$R_{o\ eq}\% = 0.28\ R_{o\ org}\% + 1.03$ (when $R_{o\ org}\% > 0.75$, Xianming et al., 2000, Eq. 2)

$R_{o\ eq}\% = 0.73\ R_{o\ org}\% + 0.16$ (Petersen et al., 2013, Eq. 3)

$R_{o\ eq}\% = 0.9916\ R_{o\ org}\% + 0.1590$ (when $R_{o\ org}\% < 0.75$, Schmidt et al., 2015, Eq. 4)

$R_{o\ eq}\% = 0.9046\ R_{o\ org}\% + 0.3786$ (when $R_{o\ org}\% > 0.75$, Schmidt et al., 2015, Eq. 5)

where $R_{o\ org}$% stands for organoclast reflectance.

3.2.4. Raman spectroscopy on kerogen

Raman spectroscopy is a powerful and promising tool for the analysis of dispersed organic matter in metamorphism and diagenesis (Beyssac et al., 2002; Guedes et al., 2010, 2012; Lahfid et al., 2010; Liu et al., 2012; Wilkins et al., 2014). It is based on the inelastic light scattering process in which the frequencies of the scattered photons are shifted from those of the incident photon frequencies according to the vibrational modes of the molecule or atomic group (Dubessy et al., 2012).

Raman spectrum on dispersed organic matter is composed of two main bands (D and G), associated with disordered and ordered structures in the organic matter respectively, and other minor bands (D2, D3, D4 according to Lahfid et al., 2010; Gl, Dl, Dr and S; according to Li, 2007) whose occurrence depends on the degree of structural ordering. The shape of Raman spectra changes as a response of the increase in maturation caused by the increase in paleotemperatures during progressive burial. In detail, these changes can be quantified by the intensity ratio of the D and G bands during graphitization (Ferrari and Robertson, 2000, 2004; Wopenka and Pasteris, 1972), whereas in epizone, anchizone and diagenesis, successful parametrization has been found using the area ratio of the two main bands and the minor bands (Beyssac et al., 2002; Guedes et al., 2010; Lahfid et al., 2010).

Raman analyses of Cambrian samples were performed on kerogen using a Jobin Yvon micro-Raman LabRam system in a backscattering geometry, in the range of 700–2300 cm^{-1} using a 600 grooves/mm spectrometer gratings and CCD detector under a maximum of 100× optical power.

A Neodimium-Yag laser source with a wavelength of 532 nm (green laser), power of <0.4 mW, and spot of 2 μm (with a 50× objective) was used during measurements. The Raman backscattering was recorded after an integration time of 20s for 6 repetitions for each measurement.

Spectra were deconvoluted using LabSpec software in order to determine frequencies, band widths and band intensities. Two different deconvolution approaches were applied as samples pertain to different levels of thermal maturity. For anchizone conditions, Raman spectra are deconvoluted using a pure Lorentzian five peaks curve-fitting according to Lahfid et al. (2010), whereas for diagenesis, a mixed Gaussian-Lorentzian six peaks decomposition provides the best solution (Guedes et al., 2010).

3.2.5. Palynomorph Darkness Index (PDI)

Recently Goodhue and Clayton (2010) proposed a new quantitative method to establish organic matter thermal maturity: the Palynomorph Darkness Index (PDI). It is a relatively simple method that utilizes a transmitted light microscope with digital imaging capacity and software capable of image analysis. PDI is determined for measurement of the red, green and blue (RGB) intensities of light transmitted through palynomorphs to produce a single greyscale value. Goodhue and Clayton (2010) demonstrated a progressive increase of PDI with increasing temperature, suggesting that the technique is applicable through a broad temperature range. The main advantage of the PDI method is the analytic and quantitative approach that, differently than qualitative methods such as CAI, TAI and AAI, does not strictly depend on the operator's perception of colour and consequently is not empirical. Furthermore, the estimation of thermal maturity based on optical investigation of microfossils as PDI is rather inexpensive.

For PDI analysis, organic matter was concentrated from two samples (4.4 and 5.3) using palynological standard techniques. The samples were treated by acid maceration (HCl 37% and HF 50%) and filtration of the organic-rich residue at 10 μm.

Light microscope observations were performed on palynological slides using a Leica DM 1000 microscope with Differential Interference Contrast technique in transmitted light. Images were captured with the digital microscope camera and successively processed for

PDI determination using ImageJ public domain software (imagej.net).

In this study, twenty specimens from each sample of unornamented palynomorphs (e.g., prasinophytes as Tasmanites spp.) were considered for determination of PDI (i.e. PDI Tasmanites, Fig. 9). The measuring area of approximately 50 μm^2 was used with a 100× magnification. For each palynomorph, the RGB intensities of 10 different areas were measured and the PDI calculated.

3.2.6. Thermal modelling

Simplified reconstructions of the burial and thermal history of the Ordovician-Devonian successions have been performed using the software package Basin Mod® 1-D (1996). The main assumptions for modeling are that: (1) rock decompaction factors apply only to clastic deposits, according to Sclater and Christie's method (1980); (2) seawater depth variations in time are assumed as not relevant, because thermal evolution is mainly affected by sediment thickness rather than by water depth (Butler, 1992); (3) thermal modeling is performed using LLNL Easy%R_o method, based on Burnham and Sweeney (1989) and Sweeney and Burnham (1990); (4) a surface temperature of 10 °C is assumed and (5) variable heat flow values through time (35 mW/m^2 from Paleozoic to Early Cretaceous with a constant increase to the present-day values of 46 and 49 mW/m^2 from 130 My onwards; Narkiewicz, 2002) are assumed.

Thicknesses and ages of stratigraphic units have been derived from either field mapping and previous papers (Kozłowski, 2008; Gągała, 2015; Trela, 2007) or from wells (see Fig. 2b for wells location; wells stratigraphy comes from: http://geoportal.pgi.gov.pl/portal/page/portal/otwory).

Burial and thermal models were constrained by organic and inorganic thermal indicators. Illite content in mixed layers I-S was converted into $R_{o\,eq}$% values using the correlations between these two indicators (Aldega et al., 2007b; Merriman and Frey, 1999).

4. Previous thermal maturity data

Thermal maturity indicators from Cambrian successions are mainly TAI data coming from Szczepanik (1997) and then presented as CAI values by Narkiewicz (2002). These data show different levels of thermal maturity for the two blocks. As a matter of fact, CAI values in the Kielce block range between 1 and 2 indicating the immature to early mature stage of HC generation, whereas they indicate the late mature and overmature stages in the Łysogóry block with CAI values ranging between 3 and 5 (Fig. 4a).

Thermal maturity of Llandovery to Ludlow graptolites-bearing shales has been estimated by CAI values (Narkiewicz, 2002), and by reflectance measurements performed on vitrinite-like macerals and graptolites (Smolarek et al., 2014). CAI values from the Kielce block show low levels of thermal maturity (1.5) in the Bardo syncline, and high levels (4), close to the HCF (Fig. 4b). Graptolites and/or other organoclasts reflectance values range from 0.7 to 1.7 $R_{o\,eq}$% (Fig. 4b; Smolarek et al., 2014) showing a general increase of thermal maturity toward the north and the northwest in the Kielce block.

Organic matter optical analyses of Devonian rocks have been widely performed in the Kielce block (Marynowski et al., 2001; Rospondek et al., 2008), whereas just one value is available for the northernmost part of the Łysogóry block (Belka, 1990). Vitrinite reflectance between 0.55 and 0.67% (Marynowski et al., 2001; Rospondek et al., 2008) indicates levels of thermal maturity consistent with the early mature stage of hydrocarbon generation for the south-western part of the Kielce block. Moving toward the NE, vitrinite reflectance ranges between 0.74 and 1.20% along the HCF.

In the Łysogóry block, only one vitrinite reflectance value of 1.15% is available (Belka, 1990).

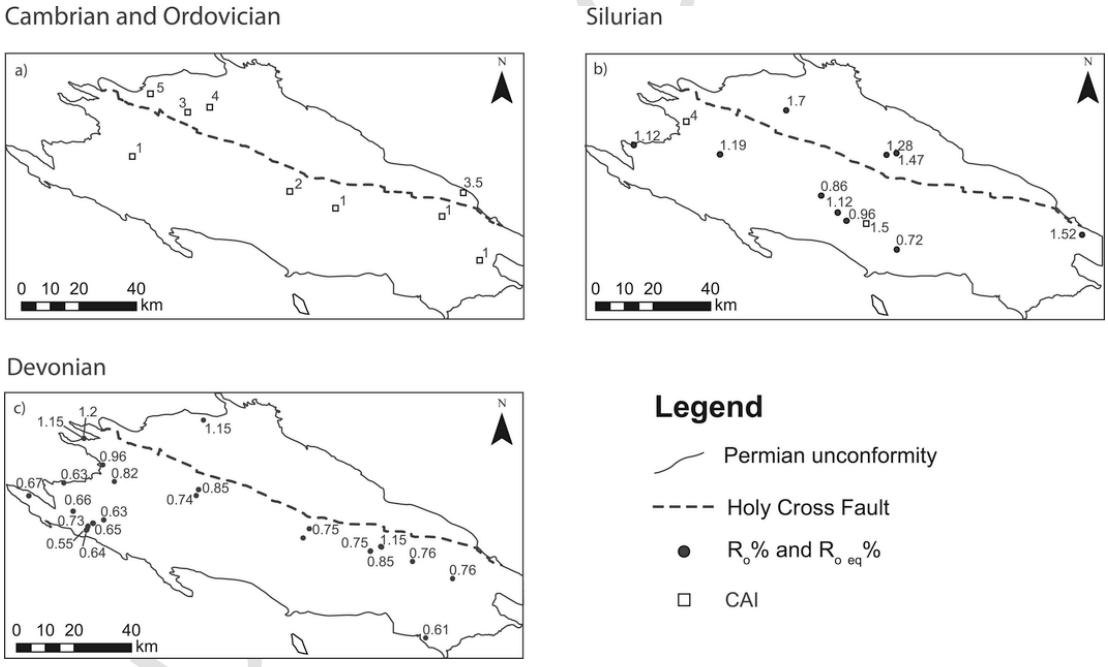

Fig. 4. Distribution of thermal maturity indicators for Cambrian-Ordovician (a), Silurian (b) and Devonian (c) stratigraphic intervals compiled after Belka (1990); Szczepanik (1997, 2001); Marynowski et al. (2001); Narkiewicz (2002); Smolarek et al. (2014). Acronyms: CAI = Conodont alteration index; R_o% = vitrinite reflectance; $R_{o\,eq}$% = vitrinite reflectance equivalent values.

5. Results

5.1. Clay mineralogy

X-ray diffraction results for the whole-rock composition and the <2 μm grain-size fraction of Cambrian to Jurassic samples are shown in Table 2 and plotted in Fig. 5.

Table 2
X–ray semiquantitative analysis of the whole rock composition and <2 μm grain size fraction for the Paleozoic to Jurassic successions. Acronyms: % I in I-S - illite content in mixed layers illite-smectite; R - stacking order of mixed layers I-S; % C in C-S - chlorite content in mixed layers chlorite-smectite; Sm - smectite; C-S - mixed layers chlorite-smectite; Rec - rectorite; I - illite; I-S - mixed-layers illite-smectite; Kln - kaolinite; Chl - chlorite; Qtz - quartz; Cal - calcite; Dol - dolomite; Kfs - K- feldspar; Pl - plagioclase; Ph - phyllosilicates; Sid - siderite; Py - pyrite; Hem – hematite; Ank - ankerite; Gt - goethite; Prl – pyrophyllite; N.D. – not determined. Subscript numbers correspond to mineral weight percentages. In bold: Kielce block samples; in roman: Łysogory block samples; in italics: Mesozoic samples.

Samples	Whole-rock composition	<2 μm grain size fraction	%I in I-S (R)	%C in C-S
CAMBRIAN				
7.1	**$Qtz1_3$ Pl_{10} Ph_{76} Hem_1**	**I_{72} I-S_{10} C-S_{17} Chl_1**	**77 (R1-R3)**	**55**
1.1	Qtz_{18} Kfs_2 Pl_4 Ph_{76}	I_{91} Rec_5 Chl_3 Prl_1	–	–
1.2	Qtz_{23} Kfs_1 Pl_3 Ph_{73}	I_{90} Rec_3 Kln_6 Prl_1	–	–
ORDOVICIAN				
6.1	**Qtz_{23} Pl_2 Ph_{73} Hem_2**	**I_{69} I-S_{11} Kln_{20}**	**83 (R3)**	**-**
5.4	**Qtz_{33} Kfs_1 Pl_2 Ph_{64}**	**I_{59} I-S_{20} Kln_{21}**	**83 (R3)**	**-**
SILURIAN				
19.1	**Qtz_{17} Pl_3 Ph_{74} Gt_6**	**I_{87} I-S_7 Kln_5 Chl_1**	**83 (R3)**	**-**
5.1	**Qtz_{40} Kfs_1 Pl_3 Ph_{56}**	**I_{72} I-S_{15} Chl_{13}**	**77 (R1)**	**-**
5.2	**Qtz_{31} Kfs_1 Pl_6 Ph_{62}**	**I_{74} I-S_{15} Chl_{11}**	**77 (R1)**	**-**
5.3	**Qtz_{14} Pl_7 Ph_{79}**	**I_{85} I-S_1 C-S_9 Kln_1 Chl_{14}**	**83 (R1-R3)**	**60**
4.5	**Qtz_{17} Kfs_1 Pl_7 Ph_{75}**	**I_{69} I-S_7 C-S_{17} Kln_3 Chl_4**	**83 (R3)**	**60**
4.4	**Qtz_{14} Cal_4 Kfs_1 Pl_8 Ph_{69} Py_2 Dol_2**	**I_{67} I-S_2 C-S_{10} Kln_4 Chl_{17}**	**81 (R3)**	**80**
4.3b	**Qtz_{17} Cal_5 Kfs_1 Pl_9 Ph_{67} Dol_1**	**I_{65} I-S_2 C-S_8 Kln_3 Chl_{22}**	**80 (R3)**	**80**
4.3a	**Qtz_{17} Cal_6 Kfs_1 Pl_{12} Ph_{62} Py_1 Dol_1**	**I_{66} I-S_6 C-S_9 Kln_5 Chl_{14}**	**82 (R3)**	**80**
4.2	**Qtz_{13} Cal_2 Kfs_1 Pl_{10} Ph_{74}**	**I_{55} I-S_{12} C-S_{12} Kln_4 Chl_{17}**	**83 (R3)**	**80**
4.1	**Qtz_{12} Kfs_1 Pl_8 Ph_{79}**	**I_{64} I-S_{19} C-S_{14} Kln_1 Chl_2**	**80 (R1-R3)**	**60**
13.1	Qtz_9 Pl_2 Ph_{89}	Sm_{43} I_{50} I-S_2 Chl_5	88 (R3)	–
12.1	Qtz_{16} Pl_6 Ph_{78}	I_{62} I-S_4 Chl_{34}	86 (R3)	–
12.2	Qtz_{15} Pl_6 Ph_{79}	I_{62} I-S_8 C-S_{11} Kln_4 Chl_{15}	86 (R3)	54
11.1	Qtz_5 Pl_4 Ph_{88} Hem_3	I_{83} I-S_5 Kln_{10} Chl_2	85 (R3)	–
11.2	Qtz_{15} Pl_4 Ph_{80} Hem_1	I_{79} I-S_{12} Kln_4 Chl_5	85 (R3)	–
10.1	Qtz_{15} Pl_6 Ph_{79}	I_{58} I-S_{24} C-S_{10} Kln_7 Chl_1	85 (R3)	78
DEVONIAN				
8.1	Qtz_2 Cal_{25} Ank_1 Ph_{72}	I_{76} I-S_{16} Kln_8	83 (R3)	–
16.1	**Qtz_7 Cal_{25} Kfs_1 Pl_2 Ph_{65}**	**I_{79} I-S_7 Chl_{14}**	**82 (R3)**	**-**
16.2	**Qtz_5 Cal_{52} Kfs_1 Pl_1 Ank_5 Ph_{35} Py_1**	**N.D.**	**N.D.**	**N.D.**
9.1	Qtz_9 Pl_2 Ph_{87} Hem_2	I_{59} I-S_6 Kln_{27} Chl_8	82 (R3)	–
2.1	Qtz_{10} Pl_4 Ph_{86}	I_{95} I-S_1 C-S_3 Kln_1	84 (R3)	50
15.1	**Qtz_6 Cal_{48} Pl_1 Ph_{45}**	**I_{85} I-S_{15}**	**85 (R3)**	**-**
20.1	**Qtz_2 Cal_{75} Ph_{23}**	**I_{80} I-S_{12} Chl_8**	**80 (R1-R3)**	**-**
TRIASSIC				
14.1	*Qtz_{34} Pl_2 Ph_{58} Hem_6*	*I_{78} I-S_5 Kln_{14} Chl_3*	*80 (R3)*	*N.D.*
JURASSIC				
17.1	*Qtz_{86} Ph_{14}*	*N.D.*	*N.D.*	*N.D.*
17.2	*Qtz_2 Pl_1 Ph_{97}*	*N.D.*	*N.D.*	*N.D.*
17.3	*Qtz_{15} Pl_1 Ph_{84}*	*I_{38} I-S_{26} Kln_{25} Chl_{11}*	*65 (R1)*	*-*
17.4	*Qtz_{69} Ph_{31}*	*N.D.*	*N.D.*	*N.D.*
17.5	*Qtz_{72} Kfs_1 Ph_{27}*	*N.D.*	*N.D.*	*N.D.*
18.1	*Qtz_{10} Kfs_1 Pl_4 Ph_{84} Sd_1*	*I_{15} I-S_3 Kln_{68} Chl_{14}*	*75 (R1-R3)*	*-*

Randomly oriented whole-rock powder patterns of Cambrian samples are composed of phyllosilicates and quartz with subordinate amounts of plagioclase, k-feldspar and hematite. The <2 μm grain-size fraction contains illite as major mineral and subordinate amounts of rectorite, kaolinite, chlorite and pyrophyllite. Occasionally, two populations of mixed layers illite-smectite (R1-R3 I-S with an illite content of 77%) occur in the Kielce block indicating retrograde diagenesis (Nieto et al., 2005).

Ordovician samples from the Bardo syncline, in the Kielce region, are mainly characterized by phyllosilicates (illite, mixed layers I-S and kaolinite) and quartz, which constitute 96%–97% of the overall composition. Plagioclase, hematite (in sample 6.1) and K-feldspar (in sample 5.4) occur as minor phases. Mixed layers illite-smectite are composed of long-range ordered structures (R3) with an illite content of 83%.

Silurian shales are mainly composed of phyllosilicates, quartz and minor amounts of albite. Occasionally calcite, dolomite, k-feldspar, goethite and pyrite occur in the sediments of the Kielce block and hematite in the Łysogory block. In the <2 μm grain-size fraction, clay mineral assemblage is mainly represented by illite, chlorite, mixed layers illite-smectite and chlorite-smectite and small amounts of kaolinite. Discrete smectite, when detected, is interpreted as a result of retrograde diagenesis (Nieto et al., 2005).

Mixed-layers I-S mostly consist of long-range ordered structures (R3) with an illite content between 80 and 88%. In a few cases, short range ordered I-S (R1) with an illite content of 77% were observed. Mixed layers chlorite-smectite have a chlorite content ranging from 54% to 80%.

The Devonian succession collected in the Kielce block is composed of high amounts of carbonate group minerals (calcite, dolomite and ankerite) and phyllosilicates, and subordinate amounts of quartz and albite, whereas the samples collected in the Łysogory block mostly contain phyllosilicates and occasionally carbonate minerals and albite. Oriented mounts show an illite-rich assemblage with subordinate amounts of chlorite, kaolinite and mixed layers I-S (Table 2).

Mixed layers I-S for both blocks correspond to R3 structures with an illite content between 80 and 85%.

The Triassic portion of the succession is characterized by quartz, phyllosilicate minerals and small contents of hematite and plagioclase. Among the phyllosilicates in the <2 μm grain-size fraction, an illite-rich assemblage with subordinate kaolinite contents and small amounts of long-range ordered mixed layer I-S and chlorite was observed.

Samples from the Jurassic succession are mainly composed of quartz and phyllosilicates and low amounts of K-feldspar and plagioclase. In the <2 μm grain size fraction, illite and kaolinite are the most abundant minerals followed by mixed layers I-S and chlorite (Table 2). Mixed layers I-S are R1 structures with 65% of illitic layers or R1-R3 structures with an illite content of 75%.

5.2. TOC and Rock-Eval pyrolysis

TOC measurements and Rock-Eval pyrolysis data are shown in Table 3. TOC content for most samples is generally below 1%. In particular, samples from the Łysogory block display values lower than 0.5%.

In the Kielce region, TOC contents higher than 1% are limited to the Wenlock-Ludlow, Llandoverian and Ordovician intervals collected in the Bardo syncline and from Middle Devonian rocks, where highest TOC values of about 5 and 9% were measured for samples 16.1 and 16.2.

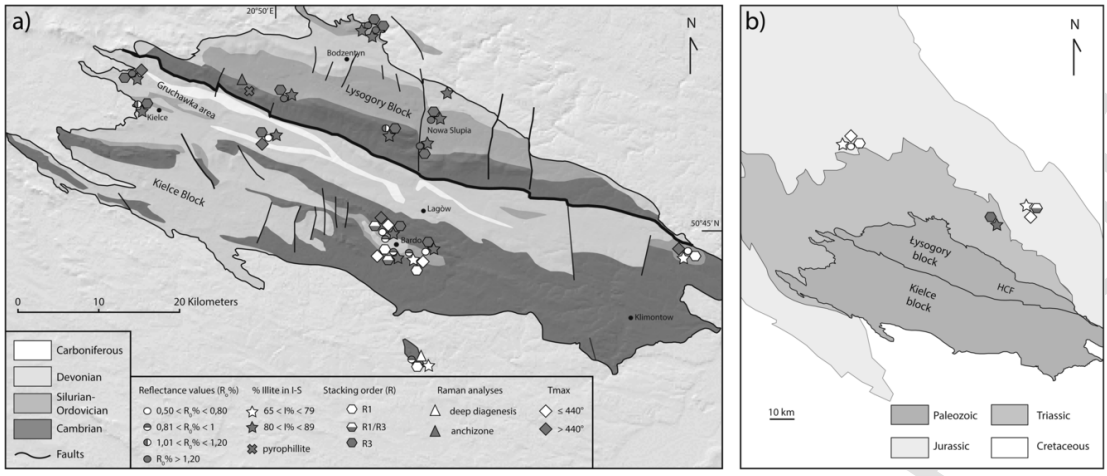

Fig. 5. Distribution of organic and inorganic thermal maturity indicators (this work) for Paleozoic (a) and Mesozoic (b) successions. Samples are labelled in Fig. 2.

Table 3
Summary of Rock-Eval Pyrolysis data. Acronyms: TOC (% in weight) – total organic carbon; HI (mg/g) – hydrogen index; T_{max} (°C): temperature at which S2 (mg/g) reaches its maximum; S1 (mg/g) = measure of volatilization of free hydrocarbons during the first stage of heating; S2 (mg/g) = hydrocarbon amount released from thermal cracking during the second stage of heating; N.D. – not determined. In bold: Kielce block samples; in roman: Łysogory block samples; in italics: Mesozoic samples.

Samples	TOC (wt%)	S1 (mg/g)	S2 (mg/g)	HI (mg/g)	T_{max} (°C)
CAMBRIAN					
7.1	**0.08**	**0.01**	**0.02**	**25**	**N.D.**
1.1	0.31	0.02	0.02	6	N.D.
1.2	0.60	0.07	0.06	10	N.D.
ORDOVICIAN					
6.1	**0.08**	**0.01**	**0.04**	**50**	**N.D.**
5.4	**2.31**	**0.03**	**2.92**	**126**	**439**
SILURIAN					
19.1	**0.82**	**0.02**	**0.53**	**65**	**442**
5.1	**2.01**	**0.09**	**4.36**	**217**	**439**
5.2	**2.04**	**0.10**	**4.28**	**210**	**437**
5.3	**1.88**	**0.09**	**2.81**	**149**	**440**
4.5	**0.81**	**0.09**	**0.84**	**104**	**441**
4.4	**1.16**	**0.16**	**1.72**	**148**	**442**
4.3b	**1.18**	**0.28**	**2.36**	**200**	**441**
4.3a	**0.93**	**0.15**	**1.35**	**145**	**441**
4.2	**0.72**	**0.10**	**0.79**	**110**	**439**
4.1	**0.50**	**0.10**	**0.41**	**82**	**441**
13.1	0.2	0.02	0.05	25	N.D.
12.1	0.09	0.02	0.02	22	N.D.
12.2	0.09	0.04	0.03	33	N.D.
11.1	0.11	0.01	0.04	36	N.D.
11.2	0.10	0.02	0.04	40	N.D.
10.1	0.13	0.01	0.01	8	N.D.
DEVONIAN					
8.1	0.23	0.01	0.05	22	N.D.
16.1	**4.57**	**0.10**	**0.41**	**9**	**N.D.**
16.2	**9.17**	**1.27**	**6.42**	**70**	**476**
9.1	0.11	0.01	0.03	27	N.D.
2.1	0.32	0.06	0.05	16	N.D.
15.1	**0.30**	**0.01**	**0.10**	**33**	**N.D.**
20.1	**0.49**	**0.03**	**0.35**	**71**	**441**
TRIASSIC					
14.1	*0.03*	*0.02*	*0.02*	*67*	*N.D.*
JURASSIC					
17.1	*0.39*	*0.01*	*0.13*	*33*	*N.D.*
17.2	*4.72*	*0.01*	*1.50*	*32*	*439*
17.3	*0.87*	*0.01*	*0.52*	*60*	*439*
17.4	*1.33*	*0.01*	*2.36*	*177*	*438*
17.5	*1.66*	*0.02*	*2.87*	*173*	*437*
18.1	*5.89*	*0.04*	*2.25*	*38*	*433*

Jurassic rocks show high TOC values with a maximum of about 6% (Table 3).

Rock Eval pyrolysis generally shows S2 values lower than 1 mg/g indicating low potential for the Cambrian to Jurassic successions except for a few samples that display values between 1.35 and 6.42 mg/g (mainly Silurian and Devonian, Table 3). S1 values are always lower than 1 mg/g except for one Devonian sample (16.2 with S1 = 1.27 mg/g).

Hydrogen indexes (HI) indicate gas prone sources ($0 < HI < 150$ mg/g) for most of samples and gas and oil prone sources ($HI > 150$ mg/g) only for three Silurian samples from the Bardo syncline (4.3b. 5.1 and 5.2) and the Jurassic section (Table 3).

T_{max} values are between 437 and 441 °C for the Ordovician-Silurian succession of the Bardo syncline, indicating the oil window, whereas the gas window was achieved only by Devonian sample 16.2 ($T_{max} > 470$ °C). Samples 19.1 (Silurian) and 20.1 (Devonian) display T_{max} values of 442 and 441 °C respectively, indicating mid mature stages of HC generation. Jurassic samples show T_{max} values between 433 °C and 439 °C suggesting the immature to early mature stage of hydrocarbon generation (Fig. 5).

Furthermore, Silurian and Jurassic kerogen is indicative of fair to good HC generation potential (Fig. 6).

5.3. Organic matter optical analysis: graptolite, vitrinite-like and vitrinite reflectance data

Results from optical analyses on dispersed organic matter of Cambrian to Jurassic samples for both tectonic blocks are shown in Table 4 and in Fig. 5.

In the Łisogory block, the kerogen of Cambrian rocks is mainly composed of vitrinite-like fragments with reflectance values ranging between 2 and 5 $R_{o\ org}$% (Fig. 7a), and rare fragments with reflectance values higher than 10 ($R_{o\ org}$%), corresponding to anthracite-graphite stages (Fig. 7b). Conversely, Cambrian rocks in Kielce block show reflectance with an average value of 1.06 $R_{o\ org}$%.

Most of measurements on Ordovician and Silurian samples in the Kielce and Łisogory blocks, were performed on small and elongated fragments recognized as graptolites (Fig. 8). These fragments show reflectance values ranging between 0.70 and 1.68 $R_{o\ org}$%%.

Devonian samples in the Kielce block close to the HCF, show very high vitrinite reflectance values ranging from 0.80 R_o% to 1.95 R_o%. Lower vitrinite reflectance values ranging from 0.84 to 1.08 R_o% were observed in the Łysogory block.

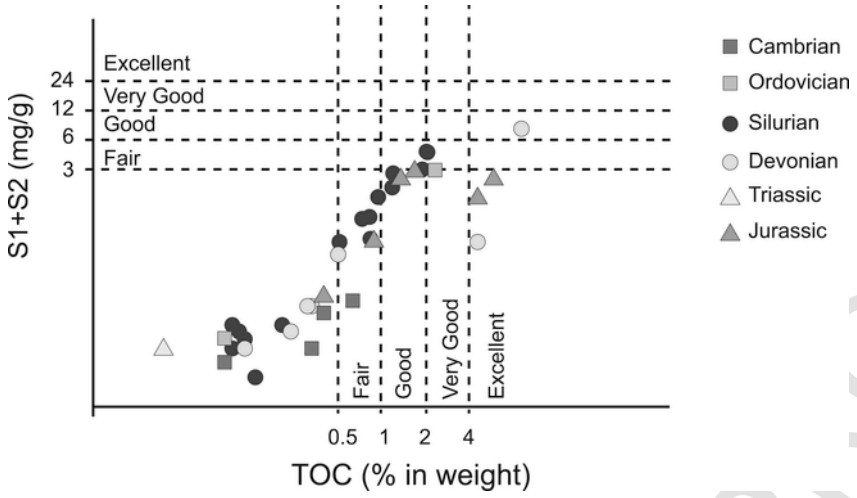

Fig. 6. S1+S2 pyrolysis data vs. total organic carbon diagram showing the petroleum source rock potential for Cambrian to Jurassic rocks.

Jurassic rocks contain vitrinite fragments with reflectance values between 0.51 and 0.57%.

5.4. PDI

In this study, only Tasmanites from two samples (4.4 and 5.3 Wenlock and Llandovery in age) were considered for PDI analysis (Fig. 9) because the other samples were barren in palynomorphs. PDI Tasmanites values were plotted on the diagram of Goodhue and Clayton (2010) suggesting paleotemperatures of about 130–135 °C. Although applied only to two samples, a cross check of the validity of this result, is provided by the corresponding R_o% value (about 0.9%) indicating the mid mature stage for HC generation.

5.5. Raman analyses on kerogen

Fig. 10 shows two representative spectra, before and after processing, for samples from the Łisogory (Fig. 10 a–b) and the Kielce blocks (Fig. 10 c–d). Spectrum in Fig. 10c has a low signal to noise ratio as a result of fluorescence that is indicative of disordered carbonaceous materials containing aliphatic chains attached to the aromatic skeleton. This evidence provides information on levels of organic matter thermal maturity, as fluorescence characterizes thermal maturity stages consistent with R_o% values lower than 1% (Quirico et al., 2005). In the spectrum of Fig. 10a, fluorescence is absent.

In detail, all spectra from the Łysogory block were fitted according to Lahfid et al. (2010) and paleotemperatures were carried out from the RA1 and RA2 parameters. RA1 parameter is the (D1 + D4)/(D1 + D2 + D3 + D4 + G) area ratio, and RA2 parameter is the (D1 + D4)/(D2 + D3 + G) area ratio (see Lahfid et al., 2010 and Fig. 10).

Results indicate that RA1 average value is 0.59 with a standard deviation of 0.009, while RA2 average value is 1.44 with a standard deviation of 0.053 (Table 5). Conversion into paleotemperatures, according to Lahfid et al. (2010), provides mean values of 268.5 °C and 260.8 °C (from RA1 and RA2 parameters, respectively) with a standard deviation of about 11 °C for both parameters (Table 5 and Fig. 10).

On the other hand for the analysis of the sample collected in the Kielce block we followed the procedure described by Guedes et al. (2010, 2012) as the method proposed by Lahfid et al. (2010) is not valid in diagensis.

After background subtraction with a third order polynomial baseline, spectra from sample 7.1 were fitted by a mixed Gaussian-Lorentzian six bands deconvolution approach (Guedes et al., 2010, 2012, Fig. 10d).

In order to obtain thermal maturity signal from Raman analyses, we calculated two parameters: the width ratio between the D and G bands (wD/wG) and the distance between the D and G bands position. The meaning of these parameters in terms of thermal maturity is described in the discussion section. As shown in Table 5, wD/wG for the spectra from the Kielce block has a mean value of 1.60 with a standard deviation of 0.049 and the distance between the D and G bands position shows an average value of 238.55 cm^{-1} with a standard deviation of 6.45 cm^{-1}.

5.6. Burial and thermal modelling

Simplified reconstruction of the burial and thermal evolution of the Kielce block has been calibrated against organoclasts reflectance, I% in mixed layers I-S and T_{max} data from the Llandovey to Ludlovian successions of the Bardo syncline (Fig. 11a).

The burial history of this succession, modelled as a pseudowell, started in deep water marine environment at about 488 My, with the deposition of 250 m thick Ordovician shales. During the Silurian, deep water sedimentation went on with the deposition of Landovery to Lower Lludlow black shales and evolved to greywackes that represent the sedimentary infill of the Caledonian foreland basin since Lower Ludlovian times (Kozłowski et al., 2014). At that time, we observed a significant increase in sedimentation rate from 0.08 mm/yr to 0.25 mm/yr. Then, the Pridolian was a period of scarce or null sedimentation as recognized by several authors (Kozłowski, 2008: Kozłowski et al., 2014; Gągała, 2015).

Sedimentation started again in Devonian times with shallow water sedimentation of sandstones during Lower Emsian that evolved in a carbonate deposition during the Lower/Middle Devonian boundary as a result of sea level rise (Szulczewski et al., 1996). The carbonate platform drowning (Szulczewski et al., 1996) occurred at the beginning of the Givetian and led to the deposition of about 700 m thick black shales during the Upper Devonian and about 400 m thick shales during the Lower Carboniferous.

Regional uplift affected the Kielce block since 310 My, as marked by the unconformity between the Cambrian-Carboniferous and the Permian successions.

Table 4
Organoclasts and vitrinite reflectance data for the Paleozoic to Jurassic successions. Acronyms: Ro org% - organoclasts reflectance; R_o%- vitrinite reflectance; $R_{o\ eq}$% - vitrinite reflectance equivalent values according to different authors; SD – standard deviation; N.D. – not determined; Nr. Meas. – number of measurements. 1 = conversion using Xianming et al. (2000) formula; 2 = conversion using Petersen et al. (2013) formula; 3 = conversion using Schmidt et al. (2015) formula. In bold: Kielce block samples; in roman: Łysogory block samples; in italics: Mesozoic samples.

Samples	$R_{o\ org}$%	SD	R_o %	SD	Nr. Meas	$R_{o\ eq}$%		
						1	2	3
CAMBRIAN								
7.1	**1.06**	**0.20**	**-**	**-**	**8**	**1.33**	**0.93**	**1.34**
1.1	>2	N.D.	–	–	N.D.	N.D.	N.D.	N.D.
1.2	>2	N.D.	–	–	N.D.	N.D.	N.D.	N.D.
ORDOVICIAN								
6.1	**0.86**	**N.D.**	**-**	**-**	**1**	**1.27**	**0.79**	**1.16**
5.4	**1.07**	**0.05**	**-**	**-**	**45**	**1.33**	**0.94**	**1.35**
SILURIAN								
19.1	**0.70**	**0.09**	**-**	**-**	**25**	**1.09**	**0.67**	**0.85**
5.1	**1.04**	**0.17**	**-**	**-**	**46**	**1.32**	**0.92**	**1.32**
5.2	**0.96**	**0.11**	**-**	**-**	**53**	**1.30**	**0.86**	**1.25**
5.3	**0.89**	**0.12**	**-**	**-**	**21**	**1.28**	**0.81**	**1.18**
4.4	**0.92**	**0.10**	**-**	**-**	**86**	**1.29**	**0.83**	**1.21**
4.5	**0.88**	**0.12**	**-**	**-**	**16**	**1.28**	**0.80**	**1.17**
13.1	**1.55**	**0.08**	**-**	**-**	**13**	**1.44**	**1.29**	**0.84**
4.3b	**0.95**	**0.14**	**-**	**-**	**89**	**1.30**	**0.85**	**1.24**
4.3a	**0.82**	**0.09**	**-**	**-**	**83**	**1.26**	**0.76**	**1.12**
4.2	**0.80**	**0.09**	**-**	**-**	**50**	**1.25**	**0.74**	**1.10**
4.1	**0.69**	**0.07**	**-**	**-**	**17**	**1.08**	**0.66**	**0.84**
11.1	N.D.	N.D.	–	–	N.D.	N.D.	N.D.	N.D.
11.2	1.62	0.08	–	–	7	1.49	1.34	N.D.
10.1	1.68	0.17	–	–	45	1.42	1.28	N.D.
12.1	1.60	0.01	–	–	3	1.48	1.33	N.D.
12.2	N.D.	N.D.	–	–	N.D.	N.D.	N.D.	N.D.
DEVONIAN								
8.1	–	–	0.84	0.14	54	–	–	–
16.1	**-**	**-**	**1.70**	**0.16**	**18**	**-**	**-**	**-**
16.2	**-**	**-**	**1.95**	**0.09**	**4**	**-**	**-**	**-**
20.1	–	–	0.80	N.D.	1	–	–	–
9.1	–	–	1.08	0.11	7	–	–	–
2.1	–	–	0.92	0.04	18	–	–	–
15.1	**-**	**-**	**1.12**	**0.02**	**2**	**-**	**-**	**-**
20.1	**-**	**-**	**0.80**	**N.D.**	**1**	**-**	**-**	**-**
TRIASSIC								
14.1	-	-	*N.D.*	*N.D.*	*N.D.*	-	-	-
JURASSIC								
17.1	-	-	*0.51*	*0.03*	*23*	-	-	-
17.2	-	-	*N.D.*	*N.D.*	*N.D.*	-	-	-
17.3	-	-	*0.57*	*0.07*	*9*	-	-	-
17.4	-	-	*N.D.*	*N.D.*	*N.D.*	-	-	-
17.5	-	-	*N.D.*	*N.D.*	*N.D.*	-	-	-
18.1	-	-	*0.57*	*0.06*	*47*	-	-	-

Sedimentation started again in Upper Permian times, continued during Triassic times with the deposition of continental and shallow marine sediments and went on during Jurassic and Cretaceous times with the deposition of about 1400 m thick limestones and marls. Maximum burial was achieved during the Late Cretaceous when the base of the Ordovician succession was buried at depths of about 6000 m.

A new uplift took place at 70 My leading to the exhumation due to erosion of about 3500 m of sediments at a rate of about 0.22 mm/yr. This event relies on the regional uplift of the Mid Polish Trough (Dadlez et al., 1994).

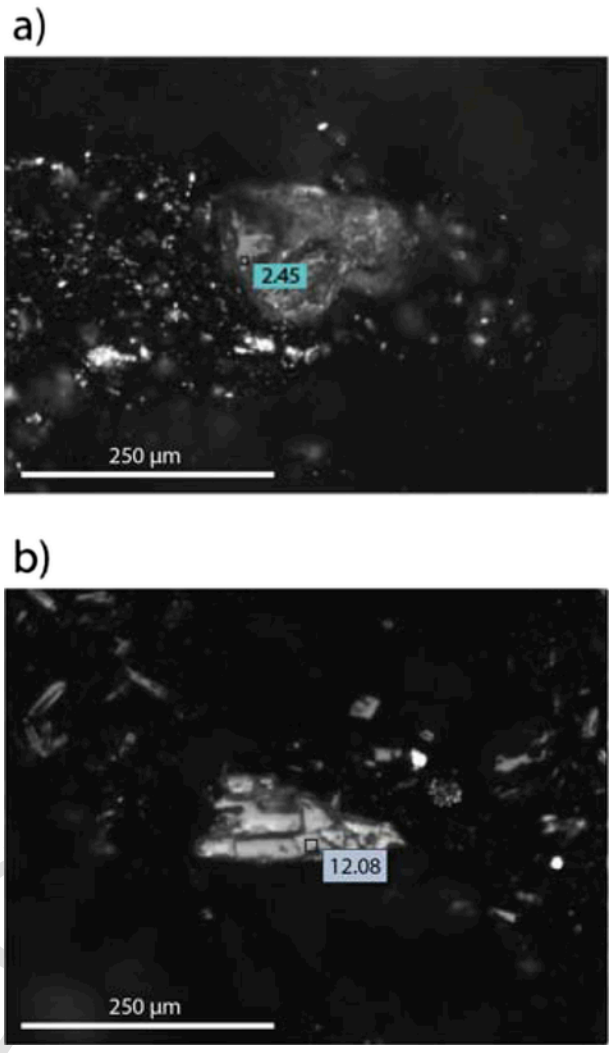

Fig. 7. Microphotographs from polished section (sample 1.1) showing high reflectance values that vary between about 2 $R_{o\ org}$%(a) and 12 $R_{o\ org}$% (b) measured on Cambrian organoclasts. Measurements have been performed on reflected light in oil immersion using a 50× objective.

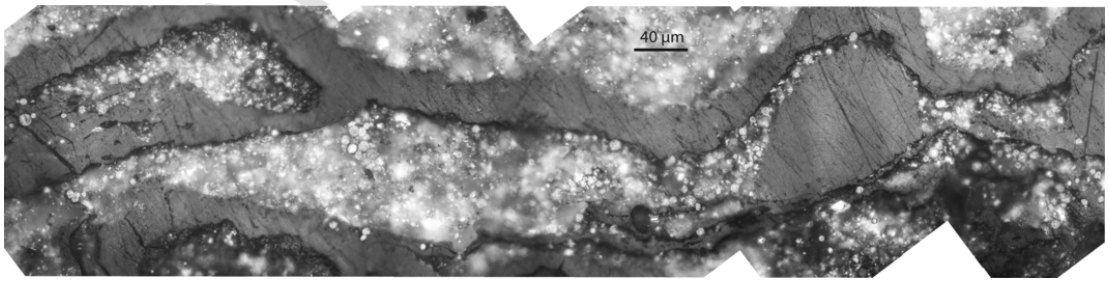

Fig. 8. Microphotograph of a graptolite fragment (sample 4.3b) in reflected light under oil immersion using a 50× objective.

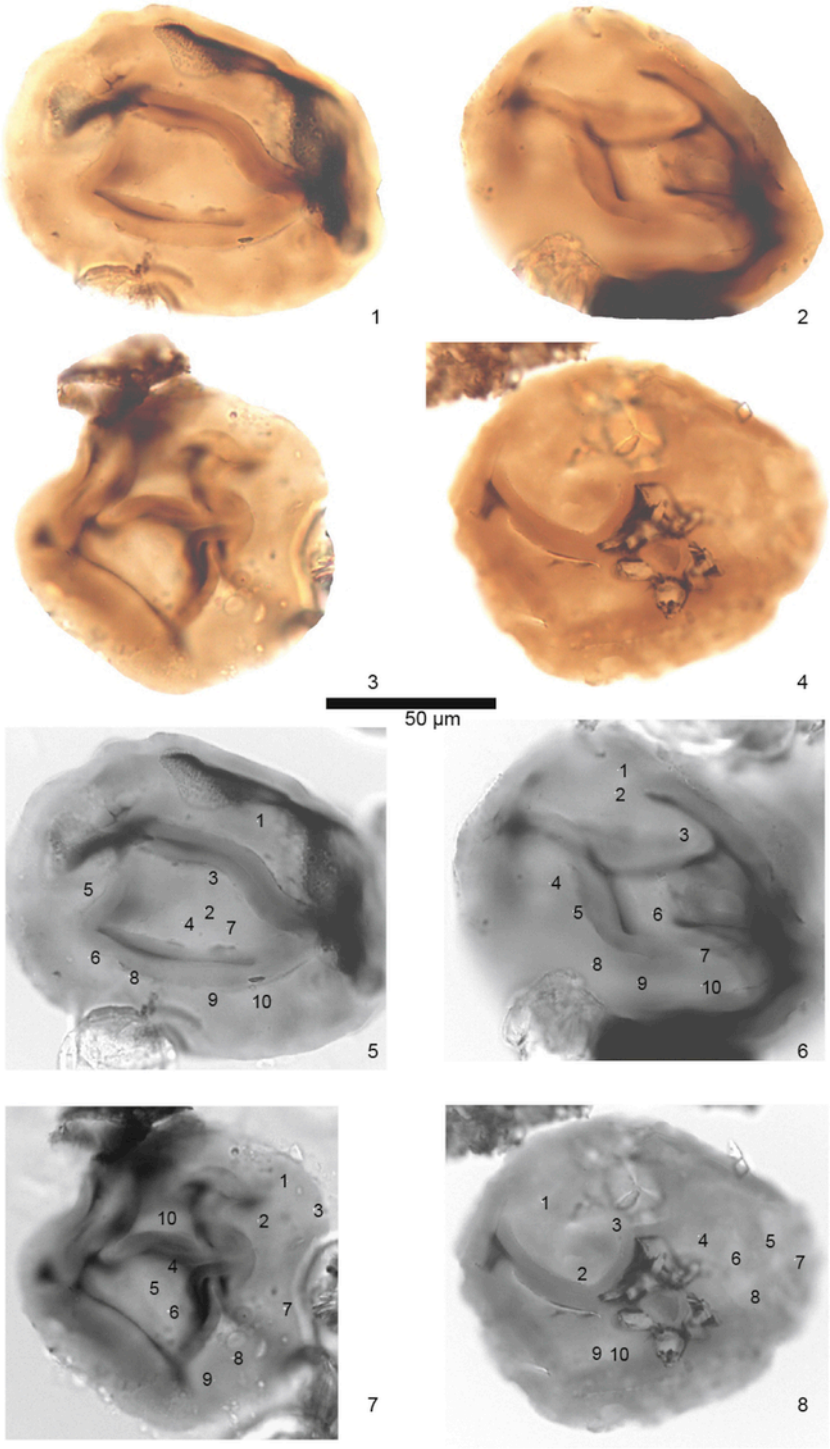

Fig. 9. Four specimens of Tasmanites selected for PDI measurements (1: slide 4.4, e.f. P38; 2: slide 4.4, e.f. T22/1; 3: slide 5.3, e.f. V28/3; 4: slide 5.3., e.f. L24/2). Each specimen (5–8) shows 10 selected areas where PDI was determined after the grey scale conversion (for further details see Goodhue and Clayton, 2010, p. 148).

The described evolution that accounts for heat flow variation through time (Fig. 11b) allows a robust calibration against organic and inorganic thermal indicators, as shown by the present-day maturity curve of Fig. 11c.

The evolutionary burial history of the Łysogory block is very similar to that previously described for the Kielce block up to the end of Late Silurian times (Fig. 12a). The first main difference is recorded at the end of Ludlovian when sedimentation went on in the Łysogory block, unlike the Kielce block, with the deposition of deep marine shales, marls and sandstones and further continued during Lochkovian and Pragian ages.

The Lower/Middle Devonian carbonate platform deposition brought to the accumulation of greater sediment thickness than that observed in the Kielce block, as well as the shales and marls deposits

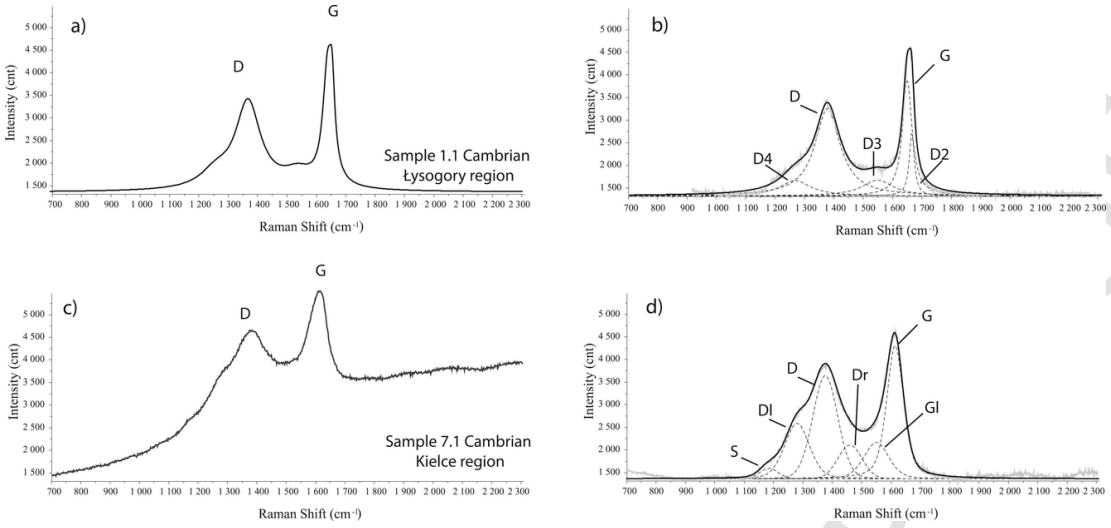

Fig. 10. Raman spectra of kerogen in Cambrian rocks. (a) Raw spectrum for sample 1.1; (b) five-peaks spectrum deconvolution according to Lahfid et al. (2010). The figure shows the bands (D, D2, D3, D4, G) used to calculate RA1 and RA2 parameters; (c) raw spectrum for sample 7.1; (d) spectrum deconvolution after baseline subtraction and a six-peaks fitting according to Guedes et al. (2010) and Schito et al. (2016b). The figure shows the position of the D and G bands and the other minor bands (S, Dl, Dr, Gl) from Li (2007) used to calculate D-G distance and wD/wG parameters.

Table 5
Mean Raman parameters obtained from the Cambrian samples in the Łysogory Block (1.1 and 1.2) and from the Lower Cambrian sample in the Kielce Block (7.1). Acronyms: RA1 = (D + D4)/(D + D2 + D3 + D4 + G) area ratio; RA2 = (D + D4)/(D2 + D3 + G) area ratio; T°C (RA1) = temperature obtained from the equation (RA1 = 0.0008T°C + 0.3758) from Lahfid et al. (2010); T°C (RA2) = temperature obtained from the equation (RA2 = 0.0045T + 0.27) from Lahfid et al. (2010); wD/wG = full width at maximum height ratio between the D and G band; D-G distance = difference between G band and D band position, in cm^{-1}; Mean = average value calculated from 10 measurements; SD = standard deviation.

Lysogory region								
	RA1 parameter		**RA2 parameter**		**T°C (RA1)**		**T°C (RA2)**	
Age of Samples	**Mean**	**SD**	**Mean**	**SD**	**Mean**	**SD**	**Mean**	**SD**
Upper Cambrian	0.59	0.009	1.44	0.053	268.46	11.03	260.80	11.8

Kielce region				
	wD/wG		**D-G distance**	
Age of Samples	**Mean**	**SD**	**Mean**	**SD**
Lower Cambrian	1.60	0.049	238.55	6.45

of the Upper Devonian, that have a maximum thickness of about 2250 m.

The Mesozoic burial was significantly deeper than that recorded by the Kielce block and was characterized by the deposition of 1200 m thick Upper Permian and Triassic sandstones, 1500 m thick Jurassic limestones and about 1500 m thick Cretaceous limestones and sandstones. This phase brought the base of the Ordovician succession at depths of about 9000 m. During the Late Cretaceous, the last uplift event eroded about 4300 m of sediments at a rate of 0.26 mm/yr.

This burial and thermal model that accounts for heat flow variation through time (Fig. 12b), allows an acceptable calibration of paleothermal data as shown in Fig. 12c. In addition, the thermal model of the Łysogory block is also consistent with vitrinite reflectance and mixed layers I-S data (R_o% on Hettangian samples between 0.51 and 0.57%, and illite content in mixed layers I-S of 75%; Tables 2 and 4) that indicate the early mature stages of HC generation.

6. Discussion

6.1. Thermal maturity of Paleozoic successions

6.1.1. Ordovician to Devonian successions

Paleozoic rocks, in particular Silurian rocks, are major gas and oil source rocks in a wide range of geological contexts (Hasany and Khan, 2003). However, the assessment of thermal maturity for lower Paleozoic rocks by means of vitrinite reflectance is limited, due to the lack of organic fragments derived from the degradation of the lignin-cellulose part of upper plants.

The use of organoclasts reflectance for Paleozoic rocks revealed to be a successfully alternative (Bertrand and Malo, 2012; Poprawa et al., 2010; Petersen et al., 2013; Smolarek et al., 2014; Suárez-Ruiz et al., 2012). Neverthless, up to now, several equations that convert grapolites measurements into vitrinite-like reflectance values have been proposed (Xianming et al., 2000; Petersen et al., 2013; Schmidt et al., 2015) but they lead to a wide range of levels of HC generation (Table 4). For this reason, we coupled organic matter optical analyses with Rock Eval pyrolysis data, Raman spectroscopy performed on kerogen and X-ray diffraction of clay minerals, in order to correlate thermal maturity indicators against different conversion for Paleozoic organic matter reflectance.

Graptolite and vitrinite-like reflectance values were calculated using three different formulas (Xianming et al., 2000; Petersen et al., 2013; Schmidt et al., 2015). As shown in Table 4, vitrinite reflectance equivalent values significantly differ from each others. In particular, formulas by Xianming et al. (2000) and Schmidt et al. (2015) provide values that are too high when compared with I% in mixed layers I-S and T_{max} values. On the other hand, vitrinite reflectance equivalent values from Petersen et al.'s formula (2013), indicate the early to mid mature stage of HC generation (R_o% between 0.66 and 0.92% for Silurian samples) that are consistent with T_{max} data (between 437 and 442) and I% in mixed layers I-S (between 77 and 83%) for samples collected at the Bardo syncline in the Kielce block (Table 1). In the Łysogory block, using the same formula, vitrinite reflectance equiva-

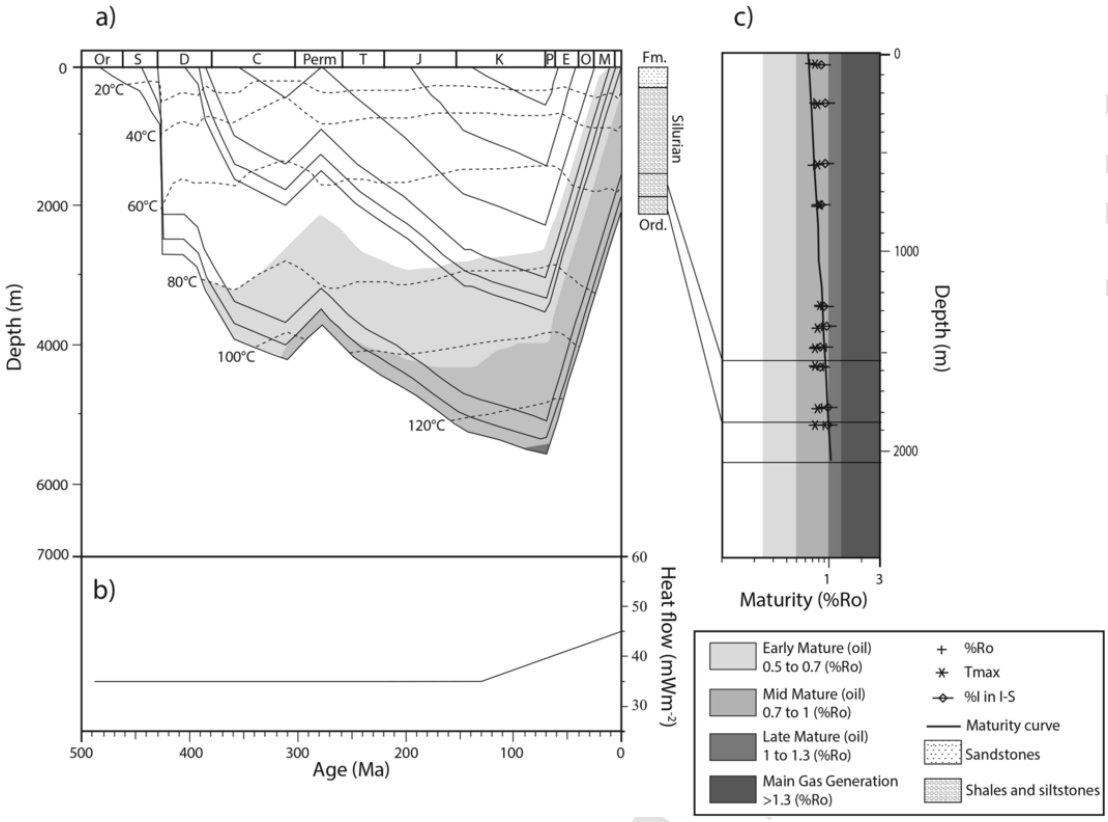

Fig. 11. (a) 1D burial and thermal history of the Paleozoic successions from the Kielce block; (b) heat flow distribution through time; (c) present-day maturity curve for the Silurian interval, calibrated against organic and inorganic thermal indicators.

lent values, between 1.28 and 1.34%, correspond to higher I% in mixed layers I-S that are proper of the first stage of gas generation.

Based on these assumptions, we applied Petersen et al.'s equation (2013) to convert organoclasts reflectance values into vitrinite reflectance equivalent data.

Obtained thermal maturity data indicate a marked difference in thermal maturity for Ordovician to Devonian samples, between the Łysogory and Kielce blocks, in agreement with previous works (Marynowski et al., 2001; Narkiewicz, 2002; Rospondek et al., 2008; Smolarek et al., 2014; Szczepanik, 1997, 2001). In detail, data distribution traces a jump between the thermal maturity of the Kielce and the Łisogory blocks from the early-late mature to mid mature-overmature, respectively.

Nevertheless, these differences cannot be appreciated in the Devonian samples in the northwestern sector of the Kielce block, where T_{max}, R_o% and I% in I-S data display higher levels of thermal maturity than those found by Rospondek et al. (2008), Marynowski et al. (2001) and Narkiewicz (2002) which are, anyway, unusually higher than values of the remaining Kielce block. According to Narkiewicz (2002), this area is a part of the Łysogory block rather than the Kielce one. Field evidences in the Mogiłki quarry near Kielce (Fig. 2) suggest intense deformation characterized by reverse folds and thrusts that can be the cause of thermal maturity increase (Caricchi et al., 2015). Thrusting related to the Holy Cross Fault movement in the latest Silurian-earliest Devonian (Late Caledonian deformation, Gągała, 2015) would have probably generated a tectonic loading which affected thermal maturity. This piece of evidence is strengthened by the repeated Carboniferous strata in the stratigraphy of the Piekosow 1 well (Fig. 2b, see for stratigraphy: http://geoportal.pgi.gov.pl/portal/page/portal/otwory).

6.1.2. Cambrian succession

Data from the Cambrian successions show that: 1) in the Łysogory block, samples experienced paleotemperatures consistent with anchizone conditions, as confirmed by the occurrence of pyrophyllite in the <2 μm grain size fraction and by Raman analyses on dispersed organic matter that display paleotemperatures between 260 and 268 °C; 2) in the Kielce block, lower levels of thermal maturity in deep diagenetic conditions as indicated by vitrinite reflectance equivalent value of 0.93% and mixed layers I-S (R1-R3 structures) were observed. Raman parameters carried out on sample 7.1 in the Kielce block, do not provide a straightforward solution in terms of paleotemperatures or levels of thermal maturity because an univocal parametrization between Raman parameters and thermal maturity in diagenesis has not been yet defined.

Different correlation between Raman parameters and thermal maturity exists in diagenesis (Kelemen and Fang, 2001; Guedes et al., 2010; Liu et al., 2012; Zhou et al., 2014; Hinrichs et al., 2014; Mumm and Inan, 2016 and Schito et al., 2016b). Nevertheless all the calculated parameters strongly depend on laser wavelength, fitting procedure and organic matter composition (Castiglioni et al., 2004; Ferrari and Robertson, 2000, 2004; Nestler et al., 2003; Pócsik et al., 1998; Schito et al., 2016b). Among them, we can compare our data only with the works of Liu et al. (2012) and Schito et al. (2016b) because:

i) They use a laser with similar wavelength (532 cm^{-1});
ii) They proposed a correlation against thermal maturity that includes Paleozoic organic matter.

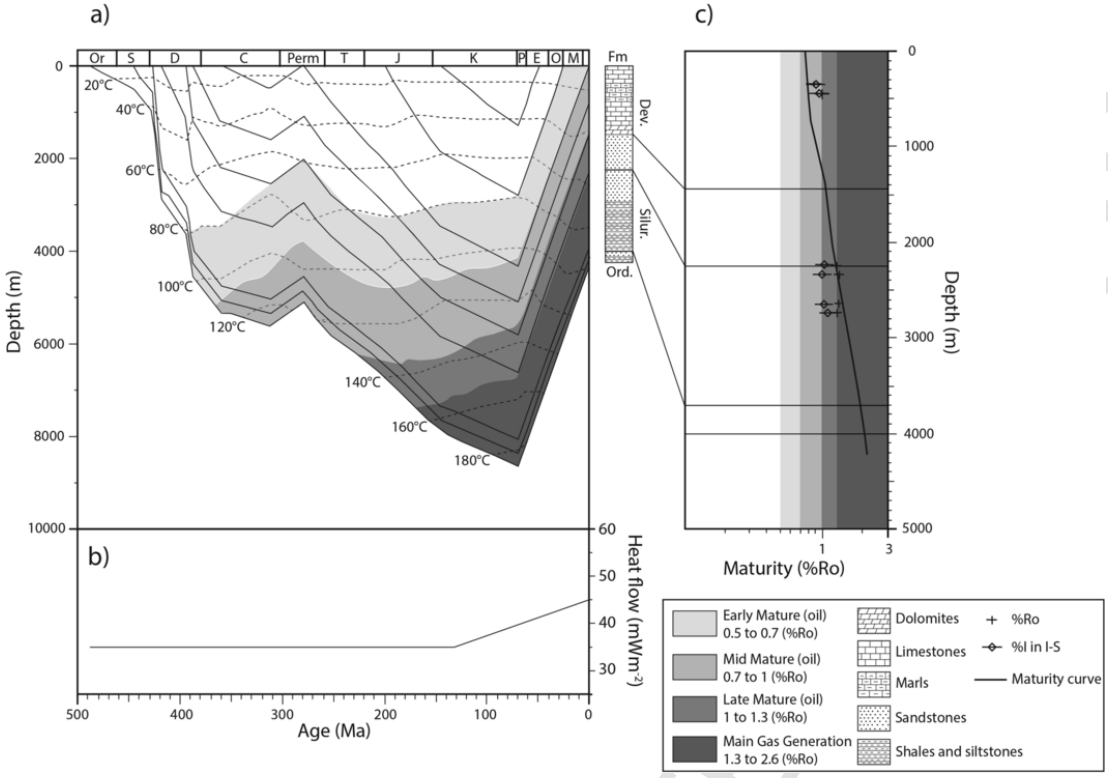

Fig. 12. (a) 1D burial and thermal history of the Paleozoic successions from the Łysogory block; (b) heat flow distribution through time; (c) present-day maturity curve for the Silurian and Devonian intervals, calibrated against organic and inorganic thermal indicators.

In Fig. 13a and b, the correlation between the wD/wG ratio parameters and R_o% from Schito et al. (2016b) and the correlation between the distance of the D and G peaks and R_o% proposed by Liu et al. (2012) are shown. On these graphs we plotted the wD/wG and the D-G distance measured on the spectrum of sample 7.1 on the y axes as light grey areas, whose widths represent the standard deviation of data.

As shown in Fig. 13a, the projection of the wD/wG parameters found in this work on the data cluster from Schito et al. (2016b) indicate a thermal maturity range between abut 1 and 1.35 R_o%, as marked by the dashed lines (Fig. 13a). In Fig. 13b, the values of the D-G distance correspond to about 1.2–1.8 R_o% (dashed lines in Fig. 13b).

Therefore, even if Raman parameters on Cambrian rocks cannot be precisely correlated to vitrinite reflectance data, they suggest a thermal maturity typical of the late mature stage of hydrocarbon generation and the initial gas generation (between about 1.0 and 1.8 R_o%) on the basis of existing literature. This evidence is also consistent with results provided by the thermal modelling performed for the successions cropping out in the Bardo syncline, according to which the base of the Ordovician interval entered the late mature stage of hydrocarbon generation during the Late Cretaceous.

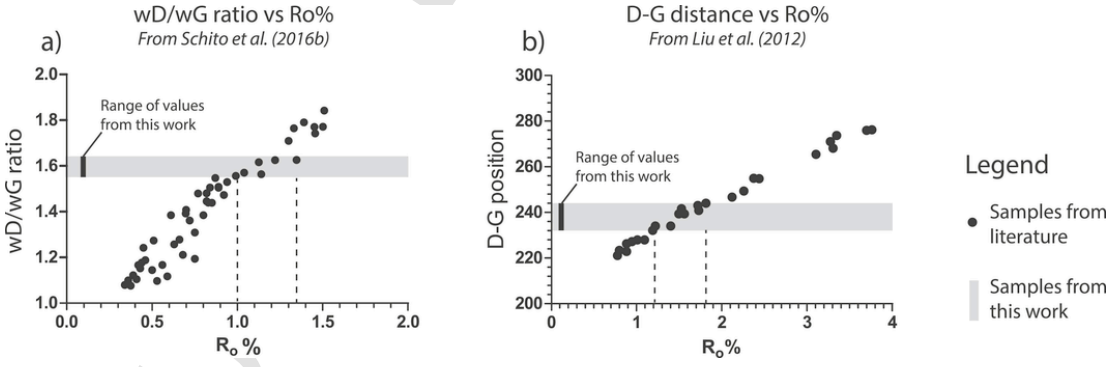

Fig. 13. (a) Comparison between our data and thermal maturity trend provided by Schito et al.(2016b) for the wD/wG values. Our data are indicated by the light grey area, whose width represents the standard deviation; (b) comparison between our data and thermal maturity trend provided by Liu et al. (2012) for the D-G distance values. Our data are indicated by the light grey area, whose width represents the standard deviation. Acronyms: wD/wG = full width at maximum height ratio between the D and G bands; D-G distance = difference between G and D bands position, in cm^{-1}.

6.1.3. Distribution of thermal maturity data by integrating published and original datasets

The whole dataset composed of published and original thermal maturity data allowed us to draw three prediction maps of the HC generation stages for Cambrian to Devonian stratigraphic intervals (Figs. 14 and 15).

Interpolation was performed by the Kernel smoothing tool in ArcGis that allows to quantify the variation of spatial distribution of data using semivariograms and predict thermal maturity in areas where data are not available, taking into account tectonic discontinuities (e.g., HCF). Devonian successions experienced levels of thermal maturity in the early and/or mid-mature stages of HC generation in the Kielce block except for a restricted area located to the northwest, close to the HCF where higher R_o% values were recorded. In the Łysogory block, levels of thermal maturity are consistent with the mid and late mature stage of HC generation even if the paucity of data and their distribution do not provide satisfactory reliability to the prediction map (Fig. 14a).

Fig. 14b shows that thermal maturity for Silurian successions in the Kielce block ranges between the early mature and the late mature stages of HC generation with a general increase from the south to the north. In the Łisogory block published and original data suggest a higher thermal maturity consistent with the gas generation stage.

The prediction map illustrated in Fig. 15a was drawn using only published data from CAI analysis (Narkiewicz, 2002) as original data are grouped in small areas and do not allow to run an acceptable interpolation. CAI data and associated HC generation windows show a general increase of level of thermal maturity from the early mature stage (southern part of the Kielce block) to the gas generation stage in the Łisogory block.

Actually, this interpolation is questionable for the Kielce block because:

(i) the overlying Silurian and Devonian successions pointed out higher levels of thermal maturity (Fig. 14a and b), and (ii) is not consistent with our spectroscopic and optical analysis of kerogen that indicate the mid to late mature stages of HC generation for the southern part of the Kielce block (R_o% = 0.79, 0.93 and 0.94% and Raman spectra correlable with vitrinite equivalent values higher than 1%) and with mixed layers I-S that highlight deep diagenetic conditions.

On the basis of our data and the prediction maps of the overlying stratigraphic intervals, we would expect levels of thermal maturity ranging from mid to late mature stages of hydrocarbon generation (Fig. 15b).

On the other hand, Raman analyses on dispersed organic matter for the Łisogory block are consistent with CAI data (higher than 3), indicating the overmature stage of HC generation (Fig. 15b).

6.2. Thermal modelling

The main points to be analysed when discussing a burial and thermal model are: 1) the reliability of thermal maturity indicators, already discussed in the previous paragraphs; 2) the thickness of the stratigraphic intervals used to build up the pseudo-wells and 3) the heat-flow distribution through time.

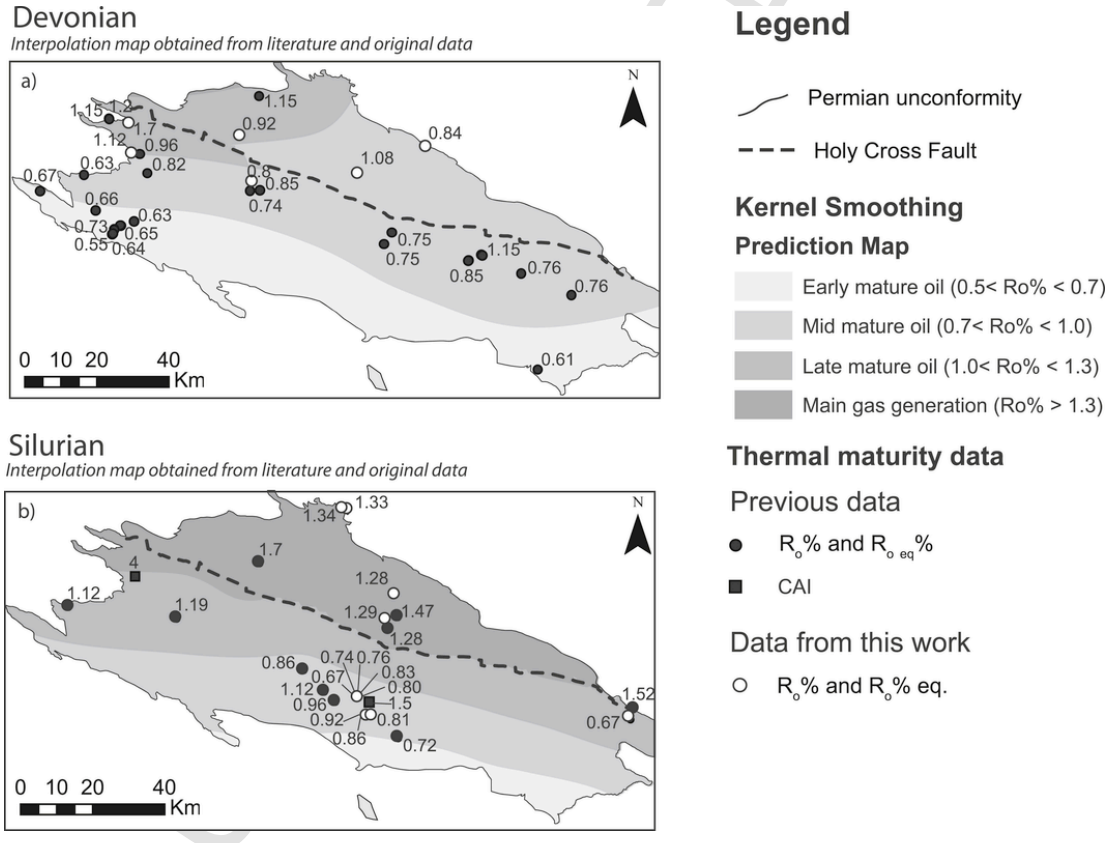

Fig. 14. (a) Prediction map for thermal maturity of Devonian successions derived from original (white dots) and published data (Belka, 1990; Marynowski et al., 2001; Rospondek et al., 2008; dark dots); (b) Prediction map for thermal maturity of Silurian successions derived from original (white dots) and published data (Narkiewicz, 2002; Smolarek et al., 2014; dark dots and black squares).

Thicknesses used to simulate the burial history of the two pseudo-wells are present day thicknesses preserved in several wells and are consistent with previous works (Gągała, 2015; Kozłowski, 2008; Narkiewicz, 2002). On the other hand, the amount of burial related to the late phases of the Variscan orogeny is still poorly constrained and needs to be further discussed. In the Kielce block, the amount of sediments deposited during the Lower Carboniferous is constrained by the Galezice G-5 well, located a few kilometres to the west of Kielce town (Fig. 2b), while the same stratigraphic interval was totally eroded in the Łysogory block. Farther to the North, Lower Carboniferous rocks can be found in the Ostalow PIG-2 well (Fig. 2b) with a thickness of about 400 m.

Kutek and Głazek (1972) and Narkeiwicz and Narkeiwicz (2010) suggest that thermal maturity of the Paleozoic successions could have been acquired during the Late Paleozoic (Late Carbonifeours-Early Permian). Nevertheless, a simulation of thermal maturity evolution as a response of Late Paleozoic burial in the Łysogory region would have implied an amount of about 6 km of sedimentary loading that is difficult to explain during a period characterised by compressional tectonics and chain exhumation, at least since Late Carboniferous times (Lamarche et al., 2002, 2003). Indeed, Narkiewicz (2002), Narkiewicz and Narkiewicz (2010) proposed a heat flow increase at the end of Paleozoic to justify their burial model, but this hypothesis is not consistent with our data for two reasons:

1) the thermal maturity curve fits Silurian paleothermal indicators from the Kielce block only with a heat flow value of 35 mW/m^2 during the Carboniferous, much lower than the present-day one (about 45 mW/m^2), when using present-day thicknesses of Paleozoic and Mesozoic successions;
2) the thermal maturity curve fits Devonian and Silurian data (Fig. 11 c) only with a burial of about 4000 m during the Mesozoic rather than assuming an increase of heat flow in the Łysogory block at the end of Paleozoic.

In conclusion, burial and thermal models proposed in this work, show that the Kielce and Łysogory blocks experienced two main events of burial characterized by large differences in sedimentation rates during upper Silurian-lower Devonian and Mesozoic times, followed by two exhumation events with different rates that partially eroded the successions. These burial and exhumation events of different magnitude can be related to the Holy Cross Fault polyphase activity. This model is consistent with Schätz et al. (2006) that, on the basis of paleomagnetic data, suggest that no large scale tectonic horizontal translation were recognized in Lower Paleozoic times, rejecting the hypothesis of a different provenance of the Kielce and Łysogory blocks proposed by Narkiewicz (2002) and Dadlez et al. (1994).

6.3. Timing of HC generation and source rock evaluation

Thermal maturity indicators derived from the organic and inorganic fraction of sediments indicate differences in levels of thermal maturity for the Paleozoic successions exposed in the Kielce and Łysogory blocks, consistent with gas generation stages in the Łysogory block and oil generation stages in the Kielce block, except for its northwestern sector.

What is important to stress, in view of the exploration of Paleozoic source rocks, is the timing of HC generation, whose effect is crucial in the evaluation of the organic matter conversion rate (Gretener and Curtis, 1982) and for modeling the migration of HC resources during the geological evolution of a basin.

Both thermal models indicate that maximum burial for the Łysogory and Kielce blocks was attained in Maastrichtian times. Furthermore our models indicate that the Ordovician to Upper Silurian successions entered the early mature stage of hydrocarbon generation between 390 and 360 My in the Kielce block, and between 390 and 380 My in the Łysogory block. The Ordovician section of the Kielce block entered the mid-mature stage between 320 and 300My, while the Ordovician, Lower Silurian and the lower part of the Upper Silurian section in the Łysogory block experienced similar hydrocarbon generation stages between 370 and 350 My ago (Fig. 11a and 12a). Moreover, Ordovician to Upper Silurian successions in the Łysogory block entered the late mature stages of hydrocarbon generation between 220 to 180 My and experienced the gas generation stage in a time that spans between 160 and 70 My (Fig. 12a).

According to our model, Lower Devonian successions entered the early mature stage of hydrocarbon generation 160 My ago in the Kielce region, while, in the Łysogory block the bottom of Lower Devonian strata entered the early mature stage of hydrocarbon generation at about 360 My, in the mid mature stage at about 200 My and in the late mature stage at 130 My (Figs. 11a and 12a).

Coupling the timing of hydrocarbon generation and the distribution of thermal maturity data for Silurian and Devonian rocks (Fig. 14a–b), with Rock-Eval pyrolysis measurements (Table 3 and Fig. 6), we can assess that the Silurian shales of the Bardo syncline and the Middle Devonian succession from the Gruchawaka area are the source rocks with the highest potential for oil generation (Fig. 6) in the Kielce block, and that the Jurassic succession is the source rocks with the highest potential in the northern area.

7. Conclusions

In this paper, we successfully face thermal maturity and source rocks assessment issues of a complex Paleozoic sedimentary succession, partially devoid of vitrinite macerals, and we reconstructed two reliable burial-thermal evolutionary models for the Holy Cross Mountains.

In detail, the main results are:

1) Organoclasts reflectance should be converted into vitrinite reflectance equivalent values by Petersen et al. 's (2013) equation as data are consistent with other thermal maturity indicators carried out from Rock Eval pyrolysis and X-ray diffraction of clay minerals;
2) Raman spectroscopy and Palynomorph Darkness Index are promising tools for assessing thermal maturity of Paleozoic organic facies;
3) Rock Eval pyrolysis and TOC analyses indicate that Silurian and Ordovician black shales cropping out in the Bardo syncline (Kielce block) and the Devonian succession from the Gruchawaka area are the most productive source rocks in the Kielce block, while the Jurassic succession is the good source rocks with the highest potential in Łysogory block;
4) Distribution maps of published and original thermal maturity data allowed us to provide a comprehensive tool for hydrocarbon exploration;
5) Differences in thickness of the sedimentary column for the Łysogory and Kielce blocks during the Silurian-Devonian interval and in Mesozoic times rely on the activation of the Holy Cross Fault as a normal fault that led to the accumulation of large amounts of sediments in the Łysogory block.

Uncited references

Beyssac et al., 2003, Caricchi et al., 201, Kowalczewski, 1974, Langford and Blanc-Valleron, 1990, Nöth et al., 2001, Urban and Gągal, 2008.

Acknowledgement

We are greatly indebted with ENI GEBA and ENI Labs for sponsoring field work and providing pyrolysis facilities. Stefano Mazzoli, Massimiliano Zattin, Benedetta Andreucci, Ada Castelluccio, Lea Di Paolo, Leszek Jankowski and Rafal Szaniawski are warmly acknowledged for passionate discussions on Polish geology and support in the field campaign. Thanks to Stefano Celano for the preliminary organisation of the dataset of existing thermal maturity data. Jan Golonka kindly contributed to discussions on Holy Cross Mts tectonic evolution. Fundings: MIUR grants to Roma Tre PhD School in Earth Sciences (XXVIII doctoral cycle).

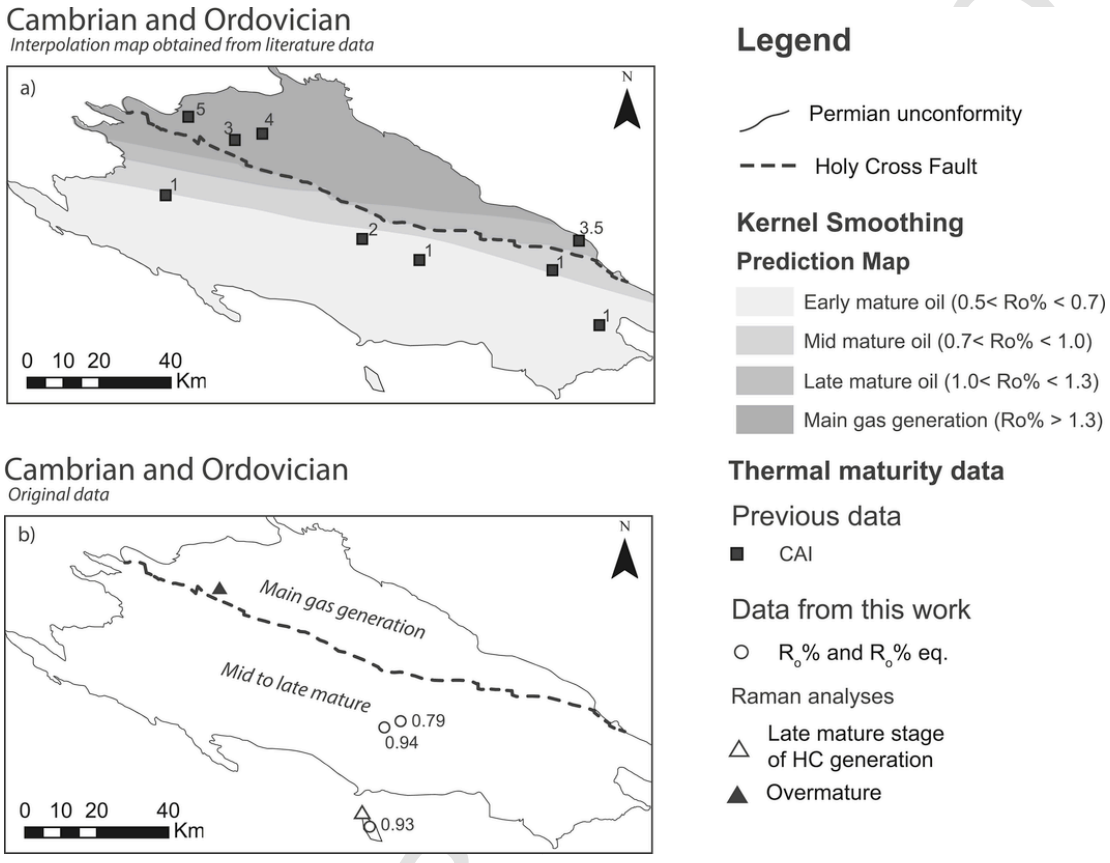

Fig. 15. (a) Prediction map for thermal maturity of Cambrian and Ordovician successions derived from published thermal maturity indicators. Data from Narkiewicz (2002) and Szczepanik (1997, 2001) are displayed as dark squares. (b) Distribution of thermal maturity indicators for the Cambrian and Ordovician successions derived from original data. Organoclasts reflectance data are indicated by white dots. White and dark triangles indicate thermal maturity derived from Raman spectroscopy (see text).

References

Aldega, L., Botti, F., Corrado, S., 2007a. Clay mineral assemblages and vitrinite reflectance in the Laga Basin (Central Appenines, Italy): what do they record?. Clays Clay Miner. 55 (5), 504–518.

Aldega, L., Corrado, S., Grasso, M., Maniscalco, R., 2007b. Correlation of diagenetic data from organic and inorganic studies in the Apenninic Maghrebian fold and thrust belt: a case study from Eastern Sicily. J. Geol. 115 (3), 335–353.

Aldega, L., Corrado, S., Carminati, E., Shaban, A., Sherkati, S., 2014. Thermal evolution of the Kuh-e-Asmari and Sim anticlines in the Zagros fold-and-thrust belt: implications for hydrocarbon generation. Mar. Pet. Geol. 57, 1–13.

ASTM D2797/D2797M-11a, 2011. Standard Practice for Preparing Coal Samples for Microscopical Analysis by Reflected Light. ASTM International, West Conshohocken, PA. http://www.astm.org/cgi-bin/resolver.cgi?D2797D2797M-11a.

AST-
MD7708-14,
Standard Test Method for Microscopical Determination of the Reflectance of Vitrinite Dispersed in Sedimentary Rocks, ASTM International, West Conshohocken, PA, 2014. www.astm.org/Standards/D7708.htm.

Barker, C., 1996. Thermal modeling of petroleum generation: theory and applications. Dev. Pet. Sci. 512.

Basin Mod® 1-D for WindowsTM, version 5.4 Software, 1996. A Basin Analysis Modelling System by Platte River Associates, Denver.

Belka, Z., 1990. Thermal maturation and burial history from conodont colour alteration data, Holy Cross Mountains, Poland. Cour. Forschungsinstitut Senckenberg 118, 241–251.

Bertrand, R., Heroux, Y., 1987. Chitinozoan, graptolite, and scolecodont reflectance as an alternative to vitrinite and pyrobitumen reflectance in Ordovician and Silurian strata, Anticosti Island, Quebec, Canada. AAPG Bull. 71 (8), 951–957.

Bertrand, R., 1990. Correlations among the reflectances of vitrinite, chitinozoans, graptolites and scolecodonts. Org. Geochem. 15 (6), 565–574.

Bertrand, R., Malo, M., 2012. Dispersed organic matter reflectance and thermal maturation in four hydrocarbon exploration wells in the Hudson Bay Basin: regional implications. Geol. Surv. Can. 7066, 54. Open File.

Beyssac, O., Goffé, B., Chopin, C., Rouzaud, J., 2002. Raman spectra of carbonaceous material in metasediments: a new geothermometer. J. Metamorph. Geol. 20 (9), 859–871.

.

Burnham, A.K., Sweeney, J.J., 1989. A chemical kinetic model of vitrinite maturation and reflectance. Geochimica et Cosmochimica Acta 53 (10), 2649–2657.

Bustin, R., Link, C., Goodarzi, F., 1989. Optical properties and chemistry of graptolite periderm following laboratory simulated maturation. Org. Geochem. 14 (4), 355–364.

Butler, R.W., 1992. Hydrocarbon maturation, migration and tectonic loading in the Western Alpine Foreland thrust belt. Geol. Soc., Lond., Spec. Publ. 59 (1), 227–244.

Caricchi, C., Aldega, L. and Corrado, S., 2015. Reconstruction of maximum burial along the Northern Apennines thrust wedge (Italy) by indicators of thermal exposure and modeling. Source Document Bull. Geol. Soc. Am., 127 (3–4), 428–442.

Caricchi, C., Corrado, S., Di Paolo, L., Aldega, L., Grigo, D., 2016. Thermal maturity of Silurian deposits in the Baltic Syneclise (on-shore Polish Baltic Basin): contribution to unconventional resources assessment. Italian J. Geosci. 135 (3), 383–393.

Carlini, M., Artoni, A., Aldega, L., Balestrieri, M.L., Corrado, S., Vescovi, P., Bernini, M., Torelli, L., 2013. Exhumation and reshaping of far-travelled/allochthonous tectonic units in mountain belts. New insights for the relationships between shortening and coeval extension in the western Northern Apennines (Italy). Tectonophysics 608, 267–287.

Castiglioni, C., Tommasini, M., Zerbi, G., 2004. Raman spectroscopy of polyconjugated molecules and materials: confinement effect in one and two dimensions. Philosophical Transactions of the Royal Society of London A: Mathematical. Phys. Eng. Sci. 362 (1824), 2425–2459.

Corrado, S., Aldega, L., Balestrieri, M.L., Maniscalco, R., Grasso, M., 2009. Structural evolution of the sedimetary accretionary wedge of the alpine system in Eastern Sicily: thermal and thermochronological constraints. Geol. Soc. Am. Bull. 121, 1475–1490.

Corrado, S., Invernizzi, C., Aldega, L., D'Errico, M., Di Leo, P., Mazzoli, S., Zattin, M., 2010a. Testing the validity of organic and inorganic thermal indicators in different tectonic settings from continental subduction to collision: the case history of the Calabria-Lucania border (southern Apennines, Italy). J. Geol. Soc. 167 (5), 985–999.

Corrado, S., Aldega, L., Zattin, M., 2010b. Sedimentary vs. tectonic burial and exhumation along the Apennines (Italy). In: (Eds.) Beltrando, M., Peccerillo, A., Mattei, M., Conticelli, S. and Doglioni, C. Geol. Italy, J. Virtual Explor. 36 (15), 1–37.

Dadlez, R., Kowalczewski, Z., Znosko, J., 1994. Some key problems of the pre-Permian tectonics of Poland. Geol. Q. 38 (2), 169–190.

Dadlez, R., 2001. Holy Cross Mts. area-crustal structure, geophysical data and general geology. Geol. Q. 45 (2), 99–106.

Dubessy, J., Caumon, M.C., Rull, F., 2012. Raman spectroscopy applied to earth sciences and cultural heritage. Mineral. Soc. G. B. Irel. 12, 83–172.

Espitalie, J., Deroo, G., Marquis, F., 1985. La pyrolyse Rock-Eval et ses applications. Revue de l'Institut Français du Pétrole 40, 563–579.

Ferrari, A.C., Robertson, J., 2000. Interpretation of Raman spectra of disordered and amorphous carbon. Phys. Rev. B 61 (20), 14095–14107.

Ferrari, A.C., Robertson, J., 2004. Raman spectroscopy of amorphous, nanostructured, diamond–like carbon, and nanodiamond. Philosophical Transactions of the Royal Society of London A: Mathematical. Phys. Eng. Sci. 362 (1824), 2477–2512.

Gągała, L., 2015. Late Silurian deformation in the Łysogóry region of the Holy Cross Mountains revisited: restoration of a progressive Caledonian unconformity in the Klonów anticline and its implications for the kinematics of the Holy Cross Fault (central Poland). Geol. Q. 59 (3), 441–456.

Goodarzi, F., Norford, B., 1987. Optical properties of graptolite epiderm-a review. Bull. Geol. Soc. Den. 35, 141–147.

Goodarzi, F., Norford, B., 1989. Variation of graptolite reflectance with depth of burial. Int. J. Coal Geol. 11 (2), 127–141.

Goodhue, R., Clayton, G., 2010. Palynomorph Darkness Index (PDI)–a new technique for assessing thermal maturity. Palynology 34 (2), 147–156.

Gretener, P.E., Curtis, C.D., 1982. Role of temperature and time on organic metamorphism. AAPG Bull. 66 (8), 1124–1129.

Guedes, A., Valentim, B., Prieto, A.C., Rodrigues, S., Noronha, F., 2010. Micro-Raman spectroscopy of collotelinite, fusinite and macrinite. Int. J. Coal Geol. 83 (4), 415–422.

Guedes, A., Valentim, B., Prieto, A., Noronha, F., 2012. Raman spectroscopy of coal macerals and fluidized bed char morphotypes. Fuel 97, 443–449.

Hackley, P.C., Cardott, B.J., 2016. Application of organic petrography in North American shale petroleum systems: a review. Int. J. Coal Geol. 163, 8–51.

Hasany, S.T., Khan, F.I.-R., 2003. Palaeozoic Sequences as Potential Source Rocks for Petroleoum in Northwestern Pakistan, with Particular Reference to the Silurian System, a Major Petroleum Source in the Middle East and North Africa Pakistan Association of Petroleum Geoscientists PAPG/SPE ANNUAL TECHNICAL. CONFERENCE 2003 Best Practices & New Technologies, Islamabad, Pakistan, 7. October 3-5, 2003.

Hinrichs, R., Brown, M.T., Vasconcellos, M.A., Abrashev, M.V., Kalkreuth, W., 2014. Simple procedure for an estimation of the coal rank using micro-Raman spectroscopy. Int. J. Coal Geol. 136, 52–58.

Hoffman, J., Hower, J., 1979. Clay mineral assemblages as low grade metamorphic geothermometers-Application to the thrust faulted disturbed belt of Montana, USA. In: Scholle, P.A., Schluger, P.S. (Eds.), Aspects of Diagenesis. vol. 2. Society of Economic Paleontologists and Mineralogists Special Publication, pp. 55–79.

Jäger, H., 2016. Optical Kerogen Analysis for Enhanced Analysis of Hydrocarbon Systems: from Mature European Basins to New Exploration in Northern Gondwana. 36. ICPSG - INTERNATIONAL CONGRESS ON "PALAEOZOIC STRATIGRAPHY OF GONDWANA" April 14-16, 2016-Perugia, Italy.

Jagodzinski, H., 1949. Eindimensionale Fehlordnung in Kristallen und ihr Einfluss auf die Röntgeninterferenzen. I. Berechnung des Fehlordnungsgrades aus den Röntgenintensitäten. Acta Crystallographica 2 (4), 201–207.

Jaworowski, K., Sikorska, M., 2006. Łysogóry unit (Central Poland) versus East European Craton-application of sedimentological data from Cambrian siliciclastic association. Geol. Q. 50 (1), 77–88.

Kelemen, S.R., Fang, H.L., 2001. Maturity trends in Raman spectra from kerogen and coal. Energy & fuels 15 (3), 653–658.

Konon, A., 2004. Successive episodes of normal faulting and fracturing resulting from progressive extension during the uplift of the Holy Cross Mountains, Poland. J. Struct. Geol. 26 (3), 419–433.

Konon, A., 2007. Strike-slip faulting in the Kielce unit, Holy Cross Mountains, central Poland. Acta Geol. Pol. 57, 415–441.

.

Kozłowski, W., 2008. Lithostratigraphy and regional significance of the Nowa Słupia group (Upper Silurian) of the Łysogóry region (Holy Cross Mountains, Central Poland). Acta Geol. Pol. 58 (1), 43–74.

Kozłowski, W., Domańska-Siuda, J., Nawrocki, J., 2014. Geochemistry and petrology of the Upper Silurian greywackes from the Holy Cross Mountains (central Poland): implications for the Caledonian history of the southern part of the trans-European Suture Zone (TESZ). Geol. Q. 58 (2), 311–336.

Kutek, J., Głazek, J., 1972. The Holy Cross area, central Poland, in the alpine cycle. Acta Geol. Pol. 22 (4), 603–651.

Kutek, J., 2001. The polish permo-mesozoic Rift Basin. Mémoires du Muséum national d'histoire naturelle 186, 213–236.

Lahfid, A., Beyssac, O., Deville, E., Negro, F., Chopin, C., Goffé, B., 2010. Evolution of the Raman spectrum of carbonaceous material in low-grade metasediments of the Glarus Alps (Switzerland). Terra Nova 22 (5), 354–360.

Lamarche, J., Mansy, J., Bergerat, F., Averbuch, O., Hakenberg, M., Lewandowski, M., Stupnicka, E., Swidrowska, J., Wajsprych, B., Wieczorek, J., 1999. Variscan tectonics in the Holy Cross Mountains (Poland) and the role of structural inheritance during Alpine tectonics. Tectonophysics 313 (1), 171–186.

Lamarche, J., Bergerat, F., Lewandowski, M., Mansy, J.L., Świdrowska, J., Wieczorek, J., 2002. Variscan to Alpine heterogeneous palaeo-stress field above a major Palaeozoic suture in the Carpathian foreland (southeastern Poland). Tectonophysics 357 (1), 55–80.

Lamarche, J., Lewandowski, M., Mansy, J.L., Szulczewski, M., 2003. Partitioning pre-, syn-and post-variscan deformation in the Holy Cross Mountains, Eastern Variscan Foreland. Geol. Soc. Lond. Spec. Publ. 208 (1), 159–184.

.

Li, C.-Z., 2007. Some recent advances in the understanding of the pyrolysis and gasification behaviour of Victorian brown coal. Fuel 86 (12), 1664–1683.

Liu, D., Xiao, X., Tian, H., Min, Y., Zhou, Q., Cheng, P., Shen, J., 2012. Sample maturation calculated using Raman spectroscopic parameters for solid organics: methodology and geological applications. Chin. Sci. Bull. 58 (11), 1285–1298.

Lopatin, N.V., 1971. Temperature and geologic time as factors in coalification. Akad. Nauk SSSR Izvestiya. Seriiya Geologicheskaya 3, 95–196.

Malec, J., Więcław, D., Zbroja, S., 2010. The preliminary assessment of the selected Paleozoic deposits of the Holy Cross Mountains. Geol. Geophys. Environ. 36 (1), 5–24.

Marynowski, L., Czechowski, F., Simoneit, B.R., 2001. Phenylnaphthalenes and polyphenyls in palaeozoic source rocks of the Holy Cross Mountains, Poland. Org. Geochem. 32 (1), 69–85.

Meneghini, F., Botti, F., Aldega, L., Boschi, C., Corrado, S., Marroni, M., Pandolfi, L., 2012. Hot fluid pumping along shallow-level collisional thrusts: the Monte Rentella Shear Zone, Umbria Apennine, Italy. J. Struct. Geol. 37, 36–52.

Merriman, R.J., Frey, M., 1999. Patterns of Very Low- Grade Metamorphism in Metapelitic Rocks. In: Frey, M., Robinson, D. (Eds.), Low Grade Metamorphism. Blackwell., Oxford, pp. 61–107.

Mizerski, W., 2004. Holy Cross Mountains in the Caledonian, Variscan and alpine cycles–major problems, open questions. Przegląd Geol. 52 (8/2), 774–779.

Moore, D.M., Reynolds Jr., R.C., 1997. X-Ray Diffraction and the Identification and Analysis of Clay Minerals. Oxford University Press, Oxford, 378.

Mumm, A.S., İnan, S., 2016. Microscale organic maturity determination of graptolites using Raman Spectroscopy. Int. J. Coal Geol. 162, 96–107.

Mustafa, K.A., Sephton, M.A., Watson, J.S., Spathopoulos, F., Krzywiec, P., 2015. Organic geochemical characteristics of black shales across the ordovician–Silurian boundary in the Holy Cross Mountains, central Poland. Mar. Pet. Geol. 66, 1042–1055.

Narkiewicz, M., 2002. Ordovician through earliest Devonian development of the Holy Cross Mts. (Poland): constraints from subsidence analysis and thermal maturity data. Geol. Q. 46 (3), 255–266.

Narkiewicz, K., Narkiewicz, M., 2010. Mid Devonian carbonate platform development in the Holy Cross Mts. area (central Poland): new constraints from the conodont Bipennatus fauna. Neues Jahrbuch für Geologie und Paläontologie-Abhandlungen 255 (3), 287–300.

Nieto, F., Mata, M.P., Bauluz, B., Giorgetti, G., Árkai, P., Peacor, D.R., 2005. Retrograde diagenesis, a widespread process on a regional scale. Clay minerals 40 (1), 93–104.

.

Petersen, H.I., Schovsbo, N.H., Nielsen, A.T., 2013. Reflectance measurements of zooclasts and solid bitumen in Lower Paleozoic shales, southern Scandinavia: Correlation to vitrinite reflectance. Int. J. Coal Geol. 114, 1–18.

Pollastro, R.M., 1990. The Illite/smectite Geothermometer- Concepts, Methodology and Application to Basin History and Hydrocarbon Generation. In: Nuccio, F., Barker, C.E. (Eds.), Society of Economic Paleontologists and Mineralogists Rocky Mountains Section. Application of Thermal Maturity Studies to Energy Exploration, Denver, pp. 1–18.

Poprawa, P., Żywiecki, M., Grotek, I., 2005. Burial and thermal history of the Holy Cross Mts. area-preliminary results maturity Model. Polskie Towarzystwo Mineralogiczne 26, 251–254.

Poprawa, P., Kosakowski, P., Wróbel, M., 2010. Burial and thermal history of the Polish part of the Baltic region. Geol. Q. 54 (2), 131–142.

Quirico, E., Rouzaud, J.N., Bonal, L., Montagnac, G., 2005. Maturation grade of coals as revealed by Raman spectroscopy: progress and problems. Spectrochimica Acta A Mol. Biomol. Spectrosc. 61 (10), 2368–2377.

Rospondek, M., Szczerba, M., Malek, K., Góra, M., Marynowski, L., 2008. Comparison of phenyldibenzothiophene distributions predicted from molecular modelling with relevant experimental and geological data. Org. Geochem. 39 (12), 1800–1815.

Sclater, J.G., Christie, P., 1980. Continental stretching: an explanation of the post-mid-cretaceous subsidence of the central North Sea basin. J. Geophys. Res. Solid Earth (1978– 2012) 85 (B7), 3711–3739.

Schätz, M., Zwing, A., Tait, J., Belka, Z., Soffel, H., Bachtadse, V., 2006. Paleomagnetism of ordovician carbonate rocks from Malopolska massif, Holy Cross Mountains, SE Poland-magnetostratigraphic and geotectonic implications. Earth Planet. Sci. Lett. 244 (1), 349–360.

Schmidt, J.S., Araujo, C.V., Souza, I.V.A.F., Chakas, R.B.A., 2015. Hydrous pyrolysis maturation of vitrinite- like and humic vitrinite macerals: implications for thermal maturity analysis. Int. J. Coal Geol. 144–145, 5–14.

Schito, A., Corrado, S., Aldega, L., Grigo, D., 2016a. Overcoming pitfalls of vitrinite reflectance measurements in the assessment of thermal maturity: the case history of the Lower Congo Basin. Mar. Pet. Geol. 74, 59–70.

Schito, A., Corrado, S., Romano, C., Guedes, A., Grigo, D., 2016b. New Raman Parameters Integrated in Classical Petroleum System Modeling to Assess Thermal Evolution of Sedimentary Basin: Four Case Histories from Cenozoic, Mesozoic and Paleozoic Sedimentary Successions. 55. ICPSG – INTERNATIONAL CONGRESS ON "PALAEOZOIC STRATIGRAPHY OF GONDWANA" April 14-16, 2016 – Perugia, Italy.

Smolarek, J., Marynowski, L., Spunda, K., Trela, W., 2014. Vitrinite equivalent reflectance of Silurian black shales from the Holy Cross Mountains, Poland. Mineralogia 45 (1–2), 79–96.

Stach, E., Mackowsky, M.Th, Teichmüller, M., Taylor, G.H., Chandra, D., Teichmuller, R. (Eds.), 1982. Gebruder Borntraeger. Stach's Textbook of Coal Petrology, Berlin, p. 535.

Suárez-Ruiz, I., Flores, D., Filho, J.G.M., Hackley, P.C., 2012. Review and update of the applications of organic petrology: Part 1, geological applications. Int. J. Coal Geol. 99, 54–112.

Sweeney, J.J., Burnham, A.K., 1990. Evaluation of a simple model of vitrinite reflectance based on Chemical kinetics (1). AAPG Bull. 74 (10), 1559–1570.

Szczepanik, Z., 1997. Preliminary results of thermal alteration investigations of the Cambrian acritarchs in the Holy Cross Mts. Geol. Q. 41 (3), 257–264.

Szczepanik, Z., 2001. Acritarchs from Cambrian deposits of the southern part of the Łysogóry unit in the Holy Cross Mountains, Poland. Geol. Quaterly 45 (2), 117–130.

Szulczewski, M., Belka, Z., Skompski, S., 1996. The drowning of a carbonate platform: an example from the Devonian-Carboniferous of the southwestern Holy Cross Mountains, Poland. Sediment. Geol. 106 (1), 21–49.

Taylor, G.H., Teichmüller, M., Davis, A.C.F.K., Diessel, C.F.K., Littke, R., Robert, P., 1998. Organic petrology: a new handbook incorporating some revised parts of Stach's textbook of coal petrology. Gebruder Borntraeger Verlagsb. 704.

Teichmüller, M., 1987. Organic Material and Very Low Grade Metamorphism. In: Frey, M. (Ed.), Low-temperature Metamorphism. Chapman & Hall, Glasgow, pp. 114–161.

Tissot, B.P., Welte, D.H., 1984. From Kerogen to Petroleum. In Petroleum Formation and Occurrence. Springer, Berlin Heidelberg, 160–198.

Tricker, P.M., Marshall, J.E., Badman, T.D., 1992. Chitinozoan reflectance: a Lower Palaeozoic thermal maturity indicator. Mar. Pet. Geol. 9 (3), 302–307.

Trela, W., 2007. Upper Ordovician mudrock facies and trace fossils in the northern Holy Cross Mountains, Poland, and their relation to oxygen-and sea-level dynamics. Palaeogeogr. Palaeoclimatol. Palaeoecol. 246 (2), 488–501.

.

Wilkins, R.W., Boudou, R., Sherwood, N., Xiao, X., 2014. Thermal maturity evaluation from inertinites by Raman spectroscopy: the 'RaMM'technique. Int. J. Coal Geol. 128, 143–152.

Wopenka, B., Pasteris, J.D., 1972. Structural characterization of kerogens to granulite-facies graphite applicability of Raman microprobe spectroscopy. Am. Mineral. 78 (5–6), 533–557.

Xianming, X., Wilkins, R.W.T., Dehan, L., Zufa, L., Jiamu, F., 2000. Investigation of thermal maturity of Lower Palaeozoic hydrocarbon source rocks by means of vitrinite-like maceral reflectance – a Tarim Basin case study. Org. Geochem. 31 (10), 1041–1052.

Zhou, Q., Xiao, X., Pan, L., Tian, H., 2014. The relationship between micro-Raman spectral parameters and reflectance of solid bitumen. Int. J. Coal Geol. 121, 19–25.